TRIBHUVAN UNIVERSITY
INSTITUTE OF ENGINEERING
PULCHOWK CAMPUS

B-06-BAS-2020/2025

INTEGRATED CONTROL SYSTEM FOR ACTIVE FIN-CONTROLLED ROCKET STABILIZATION AND GUIDANCE

By:
Manish Tajpuriya (077BAS023)
Simonkrith Lamichhane (077BAS042)
Simran Paudel (077BAS043)
Sugam Lamsal (077BAS044)

A FINAL REPORT TO THE DEPARTMENT OF MECHANICAL AND AEROSPACE ENGINEERING IN PARTIAL FULFILLMENT OF THE REQUIREMENT FOR THE BACHELOR'S DEGREE IN AEROSPACE ENGINEERING

DEPARTMENT OF MECHANICAL AND AEROSPACE ENGINEERING
LALITPUR, NEPAL

April, 2025

COPYRIGHT

TRIBHUVAN UNIVERSITY
INSTITUTE OF ENGINEERING
PULCHOWK CAMPUS
DEPARTMENT OF MECHANICAL AND AEROSPACE ENGINEERING

LETTER OF APPROVAL

The undersigned certify that they have read, and recommended to the Institute of Engineering for acceptance, a project report entitled **"Integrated Control System For Active Fin-Controlled Rocket Stabilization and Guidance"** submitted by **Manish Tajpuriya, Simonkrith Lamichhane, Simran Paudel and Sugam Lamsal** in partial fulfillment of the requirements for the Bachelor's Degree in Aerospace Engineering.

Supervisor: **Sudip Bhattarai (PhD)**, Assistant Professor
Department of Mechanical and Aerospace Engineering
Institute of Engineering, Pulchowk Campus

External Examiner: **Er. Akin Chhetri**, MEP Engineer
Kathmandu International Hospital

Head of Department : **Sudip Bhattarai (PhD**, Assistant Professor
Department of Mechanical and Aerospace Engineering
Institute of Engineering, Pulchowk Campus

DATE OF APPROVAL: 10 March, 2025

ACKNOWLEDGEMENT

This project has been prepared in partial fulfillment of the requirement for the bachelor's degree in Aerospace Engineering. First and foremost, we would like to express our sincere gratitude to Dr. Sudip Bhattrai, our project supervisor, for his constant guidance, inspiring lectures, and precious encouragement. Without his invaluable supervision and suggestions, it would have been a difficult journey for us. His useful suggestions for this work and for cooperative behavior are sincerely acknowledged.

We would like to thank the Department of Mechanical and Aerospace Engineering, Institute of Engineering, Pulchowk Campus for providing us with the opportunity of collaborative undertaking which has helped us to implement the knowledge gained over these years as a major project for the fourth year and develop a major project of our own that has greatly enhanced our knowledge and provided us a new experience of teamwork.

We acknowledge Incubation, Innovation Entrepreneurship Center (IIEC), IOE Pulchowk Campus for providing us workspace and resources.

We also would like to thank the senior and junior members of the SRB team (Nischal Shrestha, Mridul Neupane, Prashant Giri, Sunil Khadka, Prabin Bhattrai, Raju Kumar Shah, Sandesh Kunwar, Ananya Rijal, Aavash Dhakal, Bishal Karki, Mohan Yadav, Niharika Bhattrai, Rejina Timalsina and Suyasha Wasti) who have constantly helped us in doing this project. Their support has been very helpful for our project.

Any kind of suggestion or criticism will be greatly appreciated and acknowledged.

Authors:
Manish Tajpuriya
Simonkrith Lamichhane
Simran Paudel
Sugam Lamsal

ABSTRACT

Active-fin control has become a special part of space launch vehicles and military applications. This contributes to improving the accuracy and reliability of modern rockets. The main objective of this project is to develop and demonstrate the active-fins control mechanism that enhances the rocket's stability and trajectory control. In this project, real-time sensor data such as IMU and GPS has been handled using PID control algorithm to dynamically modify fin positions and guarantee desired flight routes. The project aimed to improve flight stability and trajectory accuracy. The main findings of the project are improved stability and trajectory precision.

Keywords: Active-fins control, Control algorithm, Rockets, Stability, Trajectory

TABLE OF CONTENTS

List of Figures

List of Tables

LIST OF ABBREVIATIONS

CAAN	Civil Aviation Authority of Nepal
CD	Convergent-Divergent
CFD	Computational Fluid Dynamics
CG	Centre of Gravity
CP	Centre of Pressure
DoF	Degree Of Freedom
EKF	Extended Kalman Filter
FSI	Fluid Structure Interaction
GPS	Global Positioning System
HCL	Hydrochloric acid
IMU	Inertial Measurement unit
KF	Kalman Filter
KNSU	Potassium Nitrate Sucrose
KNDX	Potassium Nitrate Dextrose
LAR	Low Aspect Ratio
LQR	Linear Quadratic Regulator
MAR	Medium Aspect Ratio
MPC	Model Predictive Control
MOHA	Ministry of Home Affairs
O/F	Oxygen Fuel
PCB	Printed Circuit Board
PID	Proportional Integral Derivative
MAR	Moderate Aspect Ratio
ULAR	Ultra Low Aspect Ratio

1. INTRODUCTION

1.1. Background

The history of rocketry dates back to ancient times, with the earliest recorded use of rockets in China during the Song dynasty (960–1279 AD) for military purposes. These early rockets were simple, unguided, and often unstable in flight. During World War II, the German V-2 rocket became the first long-range guided ballistic missile, incorporating rudimentary stabilization and guidance systems using gyroscopes and movable fins. In the present time, active fin-controlled systems have varying applications which include modern military applications like guided missiles and artillery rockets for enhanced accuracy and effectiveness. Active fin-controlled rocket stabilization and guidance is an integrated control system used to improve the flight stability and accuracy of the rocket's trajectory by dynamically adjusting the orientation of fins based on real-time flight data. This makes it useful for launching and guiding rockets to a precise trajectory that enhances the mission success rate.

1.2. Problem Statement

A rocket without an active guidance system has limited applications in real-world scenarios due to its restricted maneuverability and stringent launch conditions. However, with the integration of active control systems in the rocket, such as stability and trajectory control in our case, its potential expands significantly. The success of a rocket's mission is heavily dependent on the trajectory it follows, providing a narrow error margin. As rocket missions require extensive funding and precision, even a small error means a huge loss in mission objectives and finances. In extreme cases, even human life could be in danger due to inaccuracies. Hence, it is extremely crucial to have active stability, guidance, or both in a rocket system.

1.3. Objectives

Main Objective

To perform development and implementation of an active control systems in a sounding rocket for inflight attitude control.

Specific Objectives

- To develop a control system for the stability and guidance of a rocket.
- To ensure optimum control authority of control surfaces for rectifying lag responses.
- To perform wind tunnel and flight test of a sounding rocket with active control to assess the control authority.

1.4. Application/Features

- Guidance: The active control system can be used to guide a rocket to follow a certain trajectory.
- Satellite deployment: Guided rockets are essential for placing satellites into precise orbits around Earth, ensuring they achieve the correct altitude and orientation for their missions.
- Research: Guided suborbital rockets are used for experiments that require brief exposure to space conditions or microgravity, such as biological studies or physics experiments.
- Defense system: The active fins can be used in making missiles for defense purposes.
- Recovery: In multi-stage rockets, the first part to separate is usually the booster which can be recovered with an additional contribution of active control fins.

1.5. Feasibility Analysis

1.5.1. Economic Feasibility

Integrating active guidance systems into rockets require a substantial initial investment, but the benefits outweigh the costs. Reduced mission failure rates, the potential for re-usability, and available funding from government and private sectors provide strong financial incentives. Expenses can also be managed by making efficient material choices, streamlining design processes, and utilizing available resources. While upfront costs are high, long-term savings and increased mission success rates make this investment economically viable.

1.5.2. Technical Feasibility

The technical foundation for developing an active fins rocket is well-established. Key technologies, such as control mechanisms using servo motors and sensors like gyroscopes and accelerometers, are readily available. Consistent power supply is achievable with power management systems. Reliable real-time telemetry communication systems and simulation tools for performance optimization are also accessible. This demonstrates the strong technical feasibility of this project besides the wind tunnel which is only suitable for validation in low-velocity regions.

1.5.3. Operational Feasibility

CAAN is responsible for the safe and efficient execution of rocket activities in Nepal. It is essential to obtain regulations and permissions from CAAN for rocket operations, including a permit for a rocket launch, specifying the launch details and ensuring safety. CAAN performs a safety assessment, evaluating the trajectory path and possible impacts to identify and mitigate risks, prioritizing the safety of everyone involved.

In Nepal, MOHA is in charge of emergency management, security, and public safety. Certain laws and MOHA permits, such as security clearances for project staff to guarantee dependability and safeguard sensitive information, may be necessary depending on the project. relevant data. In order to address security concerns and put in place suitable measures, coordination with law enforcement may be required. Maintaining a safe operating environment and exhibiting a dedication to public safety and security require adherence to MOHA's safety rules, which include emergency response plans and procedures for handling hazardous materials.

1.6. System Requirements

1.6.1. Hardware Requirements

Table 1.1: Hardware Requirements

Hardware	**Applications**
Teensy 4.1, ESP32, Arduino	Micro-controllers
BNO 085, MPU6050, MPU9250	IMU sensing
Buck-Boost Converter	Volatage Regulation
Servo Motors(BMS-127WV+, Sg90)	Actuation of Fins
Load Cell	Thrust measurement
HX711	Amplifier
Li-ion/Li-Po Batteries	Power Supply
SD Card Module, SD card, Flash Chip	Data storage
LED, Buzzers	Indication system
BMP180, BMP280	Altitude Sensing
GPS Module	Navigation
LoRa Module	Communication
3D printer	Components Fabrication
Laser cutter	Cutting
Lathe Machine, CNC Machining	Nozzle Machining

1.6.2. Software Requirements

Table 1.2: Software Requirements

Software	Applications
MATLAB	Calculation, graphs
Simulink	Control System Design, Simulation and Analysis
Arduino IDE and VS code	Programming
CATIA V5, SOLIDWORKS and Fusion 360	CAD Design
Open Rocket	Rocket Design and Simulation
AeroVector	Flight Simulation and PID tuning
Ansys	Aerodynamics Simulation
RDWorks	CNC Laser Cutter
UPstudio , Bambu Studio	3D Printing

1.6.3. Material Requirements

Table 1.3: Materials Requirements

Materials	Applications
Conc. HCL, Hydrogen Peroxide	PCB Fabrication
KNO_3, Sucrose, Gun Powder, Dextrose	Propellant
Epoxy, Hardener, Cobalt, Thinner, Glass fiber	Composite Body Fabrication
Silicone Grease	Flame Protection
Mild Steel, Graphite, Cement	Nozzle Fabrication
PLA, PLA+, TPU	3D Printing
Araldite, Dendrite, Glue	Adhesive

2. LITERATURE REVIEW

Active rocket control can be achieved with the application of control surfaces and thrust vectoring. The usual control surfaces of a rocket are the canard and the fins. Any of them can be made mobile to actively guide a rocket. The major problem with canard control design is roll reversal. The canard's vortical flows alter the stabilizer surface's pressure distribution and have the potential to produce a significant rolling moment in the opposite direction. The vehicle spins in the opposite direction as the roll command when the roll reversal phenomena takes place. In this case, the control system will not function well unless this occurrence can be anticipated and taken into consideration beforehand, which calls for a lot of simulation. The amount of this induced rolling moment on stabilizers depends on some parameters such as: aerodynamics geometry, control surface deflection angle, vehicle angle of attack and flight velocity [1].

There are standard fin configurations as trapezoidal, elliptical, clipped delta, rectangular and grid. Theoretically, elliptical fins are ideal as they provide the best lifting force; however, they also produce enough induced drag to also provide drag stability to the rocket. Clipped Delta fins are primarily used on high performance rockets to yield a low drag force. The elliptical and clipped delta configurations provided more positive figures of merit compared to the other types of fins [2]. But there are many rockets that don't follow the fixed geometrical shape because of some limitations and through computational analysis they created their own configuration as Samurai Sounder [3] and Shark caved [2]. Based on the aspect ratio of the fins, three types of fins are defined; MAR, LAR and ULAR. The behaviour of MAR and LAR is similar since both types of fins generate lift mainly through circulation. On the other hand, ULAR fins generate lift due to the pressure distribution created by the wing tip or leading edge vortices, for rectangular or delta platforms respectively.[4]

The fundamental problem in model rockets is the cost of in-plant tuning, since each iteration, or flight, needs of a new motor, in addition to the risk of destroying the model in the process[4]. Because of their ease of use and good results, PID controllers are still the most widely utilized controller in rocket control systems. This is because the implementation of PID controller is fairly easy to understand, build and tune. But a common problem occurred in PID control is noise produced by any real sensor[5].

The inevitable part of any control problem is modeling the process or plant. With the advent of fast processors and numerical software like MATLAB®, Maple®, Python®, etc., it is now possible to take a complex non-linear 6-DoF equation like that of a rocket and run a program that can trim and linearize it with ease[6]. The aerodynamics of the rocket body are computed

with the Extended Modified Barrowman Equations developed by Barrowman. The actuator dynamics also have a detrimental effect in the stability of the rocket, in consequence, the actuator must also be modeled.[4]

The data received through sensors often contains significant noise, which requires real-time filtering. This is achieved through various algorithms. The ultimate goal of algorithms research is to find an optimal solution for a given problem. Although it is rare to find a completely optimal algorithm for most problem domains, one exception is Bayesian state estimation. It can be demonstrated that the Kalman Filter, an algorithm that propagates a system's fluctuating quantities over time, is the best algorithm available for its domain in this case. Fundamentally, it optimally uses linear transition functions to transmit a state with a Gaussian distribution. Since its introduction, it has mostly stayed the same due to its optimality, but it has been extended in numerous ways to apply to more than simply linear Gaussian systems. The EKF exemplifies this by linearizing nonlinear transition and observation functions using a Taylor Series expansion. [7]

Computational Fluid Dynamics (CFD) is a powerful tool in fluid dynamics that employs discretization techniques to solve governing equations at discrete points within a flow field. Initially, aerodynamic behavior was primarily analyzed using wind tunnel testing. However, with advancements in computational methods, CFD has become an integral part of the engineering design process, complementing experimental testing. Over time, CFD has evolved from being a supplementary tool to a primary resource, particularly for vehicles with a narrow flight envelope, such as missiles and model rockets [8].

CFD is highly valuable during the conceptual and preliminary design phases of a rocket, allowing engineers to assess aerodynamic performance efficiently. However, for the final design validation, wind tunnel testing remains essential. This integrated approach—leveraging CFD for design iterations and wind tunnel tests for validation—is an emerging trend that should be further encouraged to enhance the reliability of CFD-based predictions [9].

One of the critical aspects of rocket design is stability, which is significantly influenced by the fins, whether passive or active. CFD enables engineers to analyze various fin configurations and their effects on key aerodynamic parameters such as drag and lift forces. This allows for optimization of fin design to achieve the desired aerodynamic characteristics.

In this study, CFD simulations are conducted using ANSYS 2022 R1 with the Fluent solver. For inviscid flow cases, the solver applies the Euler equations, which simplify the conservation equations by neglecting molecular diffusion. While the mass conservation equation remains unchanged from laminar flow models, the momentum and energy conservation equations are reduced accordingly. This approach allows for the efficient simulation of high-speed

flows where viscosity has minimal impact, making it suitable for preliminary aerodynamic analysis.

$$\frac{\partial \rho}{\partial t} + \nabla \cdot (\rho \vec{v}) = S_m \tag{2.1}$$

$$\frac{\partial}{\partial t}(\rho \vec{v}) + \nabla \cdot (\rho \vec{v}\vec{v}) = -\nabla p + \rho \vec{g} + \vec{F} \tag{2.2}$$

$$\frac{\partial}{\partial t}(\rho E) + \nabla \cdot \left(\vec{v}(\rho E + p)\right) = -\nabla \cdot \left(\sum_j h_j J_j\right) + S_h \tag{2.3}$$

3. THEORETICAL BACKGROUND

3.1. Rocket Theory

The theory of rockets revolves around Newton's third law of motion, stating that for every action, there's an equal and opposite reaction. Rockets propel themselves by expelling high-speed exhaust gases, generated through controlled combustion of propellants. Key components include the propellant, rocket engine, nozzle, and payload. Flight dynamics involve ensuring stability, controlling trajectory, and understanding orbital mechanics during the flight. A typical flight of a model rocket can be characterized by the four phases[10]:

1. **Lift off**: A vertical launch guidance propels the rocket skyward.
2. **Thrust phase**: The rocket motor accelerates during this stage.
3. **Coast phase**: Following burnout, the rocket keeps moving upward due to inertia until it approaches its maximum altitude.
4. **Descent and recovery**: The rocket can safely return to the earth thanks to the deployment of a recovery device.

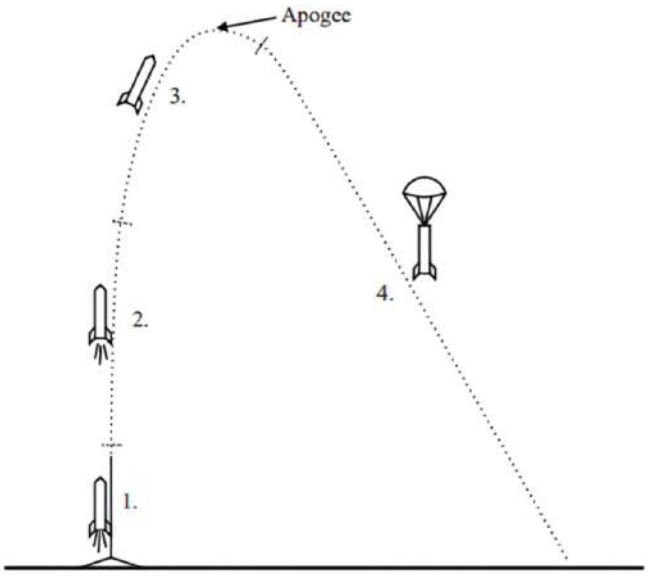

Figure 3.1: Flight Profile
[10]

3.1.1. Forces on Rocket

During flight, a model rocket experiences three fundamental forces: aerodynamic forces, gravity, and motor thrust. By expelling high-velocity gases in the opposite direction, the motors provide thrust. Typically, a rocket motor's thrust is aligned on the rocket's center axis, preventing the rocket from experiencing any angular moment. The gravitational force can be thought of as a single force coming from the CG when the forces and moments created are added up. No angular moment is produced on a body in relation to the CG by a homogenous gravitational field.
Aerodynamic forces, on the other hand, produce both net forces and angular moments. To determine the effect of the aerodynamic forces on the rocket, the total force and moment must be calculated relative to some reference point[10].

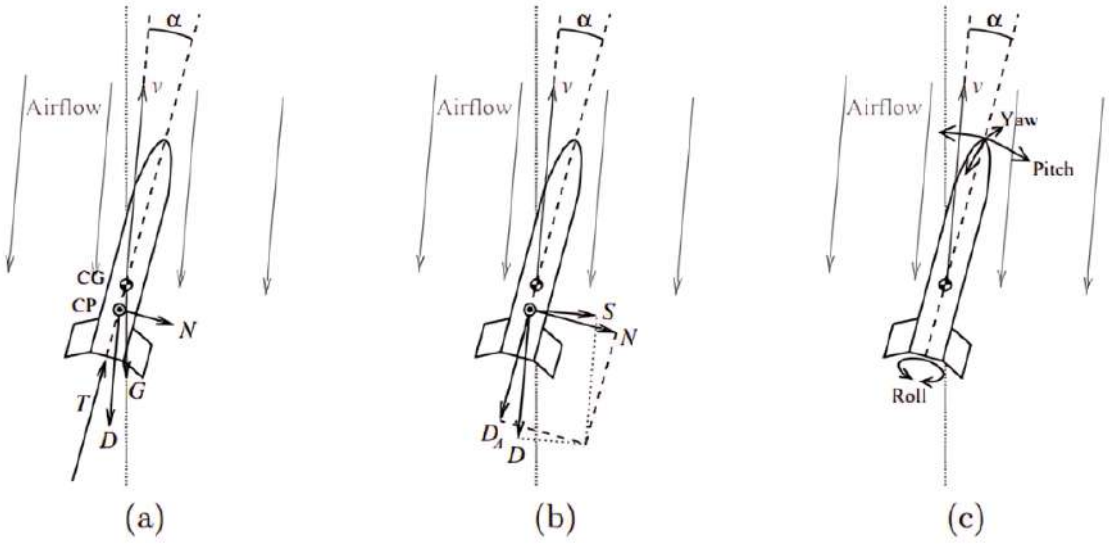

Figure 3.2: Forces acting on rocket in free flight

3.1.2. Stability of the rocket

Rocket stability is the capability of a rocket to sustain its intended orientation and path throughout flight. Ensuring stability is essential for mission success, as instability can result in erratic motion, loss of control, and mission failure.

External disturbances, such as wind gusts, can cause the rocket to deviate slightly from its original orientation. In such cases, the rocket's centerline no longer aligns with its velocity vector, creating a condition known as flight at an *angle of attack* α. Here, α denotes the angle between the longitudinal axis of the rocket and the direction of its velocity.

For a stable rocket, this angle of attack induces the fins to generate a restoring moment. This moment helps return the rocket to its intended flight path and is produced by aerodynamic forces acting perpendicular to the rocket's axis.

Each rocket component contributes its own normal force, originating from its respective center of pressure (CP), as illustrated in the diagram Figure 3.3.

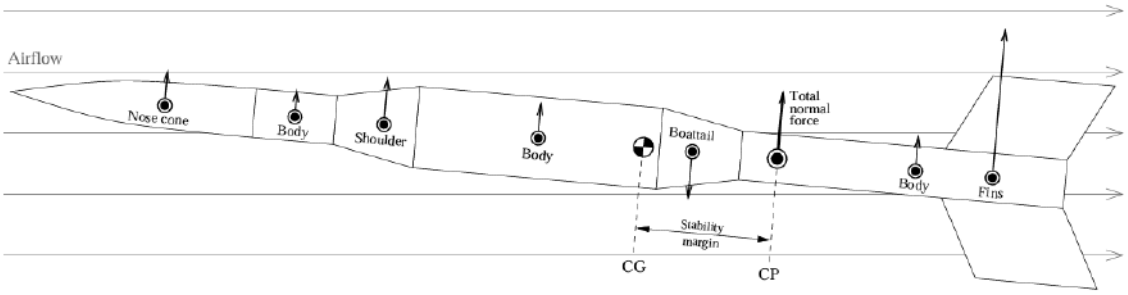

Figure 3.3: Normal forces produced by the rocket components

It is possible to combine the effects of the many normal forces into a single force, which exerts the same moment as the individual forces and has a magnitude equal to the total of the individual forces. The rocket's center of pressure is the location where the entire force acts. Only when the CP is positioned aft of the CG does the moment generated attempt to correct the rocket's trajectory, as seen in Figure 3.3. The rocket is considered statically stable if this requirement is met. When flying at a small angle of attack, a statically stable rocket always generates a corrective moment.

3.1.2.1 Static Stability: The static stability of a rocket can be defined as the tendency for a rocket to return to its original position. The behavior of the rocket and how it rotates in response to the wind is best described by the rocket's static stability margin [11].
Two circumstances could cause the above static stability argument to fall apart: First, a moment could be created with zero total force if the normal forces completely cancel each other out. Second, an uncorrective moment could result from the normal force at the CP being pointing in the wrong direction (downward in the picture). But as we'll see, a boattail is the only part that may generate a downward pull, and that force is equal to the body's corresponding broadening. As a result, neither zero nor a direction that would result in an uncorrective moment when aft of the CG may represent the whole force operating on the rocket.

There are basically three stability conditions for any body, including rockets. They are:

positive stability, neutral stability and negative stability. In positive stability, the CG is ahead of the CP; in neutral stability, the CG and CP coincides, whereas in negative stability, the CG is behind the CP. Positive stability is crucial for a rocket to ensure a controlled and successful flight, whereas neutral or negative stability can lead to unpredictable behavior or flight failure. Positioning the CG ahead of the CP and using properly sized and placed fins improves the stability ensuring a steady flight path. A commonly used criterion to quantify rocket stability is the static margin (or stability margin). [12]

$$Static\,Margin = \frac{X_{CP} - X_{CG}}{d} \tag{3.1}$$

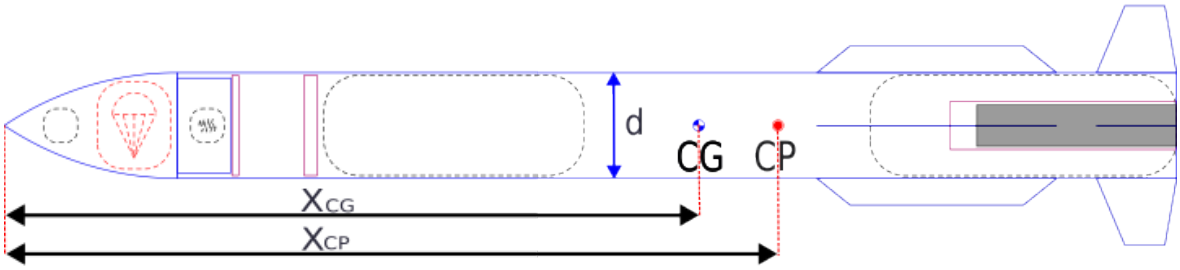

Figure 3.4: Location of CG and CP

The distance between a rocket's CP and CG, expressed in calibers—where one caliber is the rocket's maximum body diameter—is known as the stability margin. In model rocketry, it's generally accepted that the CP should be 1-2 calibers behind the CG. On the other hand, a rocket's CP usually rises as the angle of attack does. At an angle of attack of just a few degrees, a stability margin of 1-2 caliber may occasionally completely vanish. As side wind is the primary cause of angles of attack, this effect is called wind caused instability [13].

3.1.2.2 Dynamic Stability: Even a statically stable rocket might not be able to swiftly revert to its initial orientation. Model rockets may encounter several types of dynamic instability depending on their shape, size and mass.[12]. Dynamic stability refers to the rocket's behavior over time after it has been disturbed. While static stability ensures the rocket has the initial tendency to return to its original position, dynamic stability determines whether it will actually return to that position over time and in what manner. A system's dynamic response can be used to examine how it responds to a certain dynamic force. Determining the dynamic stability of any rocket is essential for a deeper comprehension of how the rocket responds to an outside disruption while in flight.

Even a rocket with statically stable performance may struggle to swiftly return to its initial orientation. Various forms of dynamic instability can affect model rockets based on their mass, size, and shape.

1. Too little oscillation damping: To put it briefly, light weight rockets may cause the perturbation to be substantially overcorrected, necessitating a corrective moment in the opposite direction. Continuous oscillation during the flight could result from this.

2. Too small corrective moment: This is an instance of over-damped oscillation, in which the rocket's moment of inertia is greater than the corrective moment. The thrust from the motors may have had a major impact on the rocket's flight path before it was able to reorient itself.

3. Roll-pitch coupling: Roll-pitch resonance might happen and make the model unstable if its natural roll frequency—which could be brought on by canting the fins, for example—is near the rocket's oscillation frequency.

   Dynamic stability problems are by definition those that develop gradually throughout the rocket's flight. The potential dynamic stability issues are also simulated using a comprehensive flight simulation that automatically accounts for all corrective moments.

3.1.3. Propellant Theory

3.1.3.1 Composition: The composition of the propellant is selected on the basis of the availability of the constituents, cost, safety, castability, performance consistency and adequate performance. Potassium nitrate serves as the oxidant, and dextrose serves as the fuel in the propellant. For KNDX, the standard ingredient ratio is 35(%) dextrose and 65(%) potassium nitrate by mass. A reasonable upper limit for "solids" loading of a sugar binder that preserves good performance and burn-rate characteristics is represented by this ratio of oxidizer to fuel mass. Although a higher O/F ratio and thus a larger "solids" loading may result in somewhat better performance, the melted mixture's (slurry's) consistency thickens. Casting becomes more challenging as a result. Lower performance and a slower burning rate are the results of using a lower O/F ratio. However, the slurry has a thinner consistency, which makes casting a bit easier. [14].

3.1.3.2 Combustion: When ignited, the dextrose-based solid propellant undergoes a rapid combustion process that releases large amounts of energy, producing hot gases that expand

and create thrust. The combustion reaction involves the oxidation of dextrose by potassium nitrate. As the dextrose burns, it breaks down into carbon dioxide (CO_2) and water vapor (H_2O), while the potassium nitrate decomposes to release oxygen, which sustains the combustion process.

The simplified chemical equation for this reaction is:

$$C_6H_{12}O_6 + 6KNO_3 \rightarrow 6CO_2 + 6H_2O + 3K_2CO_3 + \text{Energy}$$

This reaction releases significant amounts of thermal energy, which heats the gases produced (mainly CO_2 and H_2O). These gases expand rapidly under the heat, creating high pressure inside the combustion chamber. As the gases are expelled through the rocket nozzle, they generate thrust, propelling the rocket forward according to Newton's Third Law of Motion.

3.1.3.3 Burn rate: The generalization of characteristics relating to the burn rate at the specified chamber pressure, which is provided by, is another crucial propellant parameter:

$$r = \alpha.P^n \tag{3.2}$$

where the overall fluctuation of one attribute with regard to the change in another is determined by the pressure coefficient (a) and the pressure exponent (n). P stands for the combustion chamber's pressure, and r for the fuel's burn rate. Plotting the propellant's burn rate at various chamber pressures on a graph is the first step in determining the values. The values of a and n can be found by tracing the curve using the data points.

3.1.3.4 Grain Configuration: Regardless of the geometry of the perforations, a propellant grain is said to be cylindrical if its internal cross section stays constant along its axis. A propellant grain's central chambers or flow passageways are called perforations, and they can be cylindrical, tubular, rod-, or star-shaped. End burning is the most widely utilized grain type, in which the propellant burns from one end. When thrust, pressure, and burning surface area stay largely constant during motor burn time, neutral burn happens. Burn times that increase thrust, pressure, and burn surface area are referred to as progressive burning, whereas burn times that reduce these parameters are referred to as regressive burning. The proper ratios of fuel and oxidizer for full combustion are known as a stoichiometric mixture, and the oxygen balance establishes whether the propellant is over-oxidized or under-oxidized. At the end of burning, any unburned propellant remaining or expelled through the nozzle is referred to as a sliver[15].

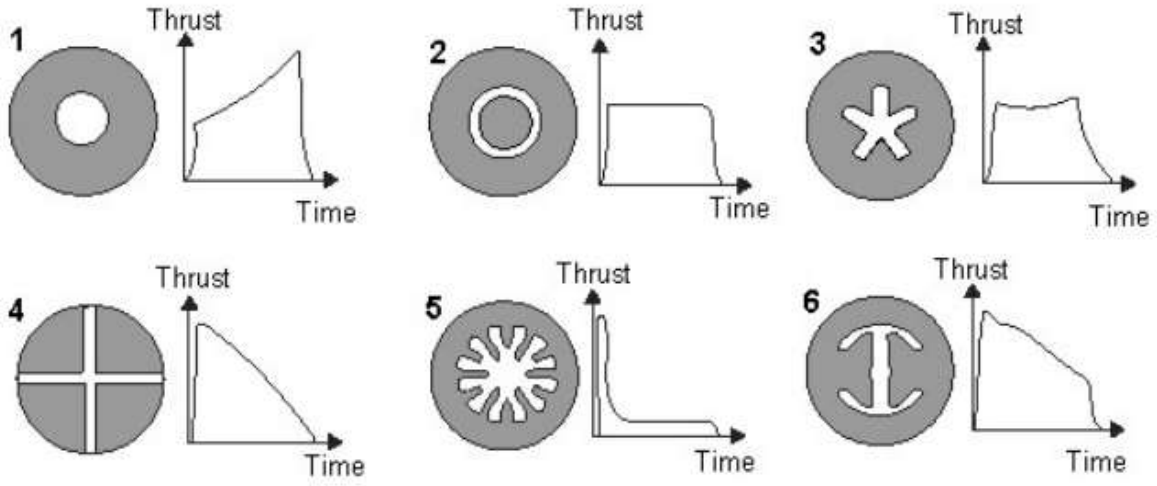

Figure 3.5: Thrust profile for different grain profiles

3.1.4. Nozzle Theory

Rocket nozzles are crucial components in rocket propulsion systems, designed to accelerate exhaust gases to produce thrust. They efficiently convert the thermal energy of combustion gases into kinetic energy, driving the rocket forward. A well-designed nozzle maximizes the thrust and overall efficiency of the rocket. Rocket engines usually have a fixed geometry CD nozzle with a much larger divergent section.

The amount of thrust produced by the rocket is given as:

$$F = \dot{m}.v_e + A_e.(p_e - p_a) \tag{3.3}$$

The exhaust velocity v_e can be derived from the energy equation for compressible flow in the nozzle, assuming isentropic expansion:

$$v_e = \sqrt{\frac{\gamma-1}{2\gamma RT_c}\left[1-\left(\frac{P_c}{P_e}\right)^{\frac{\gamma}{\gamma-1}}\right]} \tag{3.4}$$

The area ratio $\frac{A_e}{A_t}$ (exit area to throat area) is critical for achieving desired exhaust velocities:

$$\frac{A_e}{A_t} = \left(\frac{1}{M_e}\right)\left[\frac{2}{\gamma+1}\left(1+\frac{\gamma-1}{2}M_e^2\right)\right]^{\frac{\gamma+1}{2(\gamma-1)}} \tag{3.5}$$

The throat is the point where the flow transitions from subsonic to sonic, governed by:

$$\frac{A_t}{A^*} = \frac{1}{M}\left(\frac{\gamma+1}{2}\left[1+\frac{\gamma-1}{2}M^2\right]\right)^{\frac{\gamma+1}{2(\gamma-1)}} \tag{3.6}$$

where A^* represents the reference area, often equal to the throat area A_t, and M is the Mach number at any point in the nozzle.

Specific impulse measures the efficiency of the rocket engine, representing thrust per unit mass flow rate of propellant:

$$I_{sp} = \frac{V_e}{g_0} \tag{3.7}$$

3.2. Aerodynamics of model rockets

3.2.1. Aerodynamic Force Coefficients

Absolute force values are frequently challenging to interpret while researching rocket configurations since a variety of things influence them. The forces are normalized by the present dynamic pressure $q = \frac{1}{2}\rho v_o^2$ and some typical area A_{ref} to obtain a non-dimensional force coefficient that is more appropriate for comparison. Likewise, the dynamic pressure, characteristic length, and characteristic area d normalize the moments. Thus, the normal force coefficient corresponding to the normal force N is defined as

$$C_N = \frac{N}{\frac{1}{2}\rho v_o^2 A_{ref}} \tag{3.8}$$

and the pitch moment coefficient for a pitch moment m as

$$C_m = \frac{m}{\frac{1}{2}\rho v_o^2 A_{ref} d} \tag{3.9}$$

The normal force remains constant independent of the point of origin, whereas the pitch moment is always computed around a reference point. The moment coefficient at another point $C_m^{'}$ can be computed from the moment coefficient C_m if it is known for a reference point.

$$C_m^{'} = C_m d - C_N \Delta x \tag{3.10}$$

where Δx is the distance along the rocket's centerline.

The place from which the current pitching moment is produced by the total normal force alone is known as the *center of pressure* (CP). Consequently, there is no moment around the CP itself due to the total normal force, and by setting $C_m^{'} = 0$, one may derive an equation for the CP's location from (3.10):

$$X = \frac{C_m}{C_N} d \tag{3.11}$$

Here X is the position of the CP along the rocket centerline from the nose cone tip. This equation is valid when$\alpha > 0$. As α approaches zero, both C_m and C_N approach zero. The CP is then obtained as a continuous extension using L-Hospital's rule

$$X = \frac{\frac{\partial C_m}{\partial \alpha}}{\frac{\partial C_N}{\partial \alpha}} d|_{\alpha=0} = \frac{C_{m_\alpha}}{C_{N_\alpha}} d \tag{3.12}$$

where the normal force coefficient and pitch moment coefficient derivatives have been defined as

$$C_{N_\alpha} = \frac{\partial C_N}{\partial \alpha}|_{\alpha=0} \tag{3.13}$$

and

$$C_{m_\alpha} = \frac{\partial C_m}{\partial \alpha}|_{\alpha=0} \tag{3.14}$$

At very small angles of attack we may approximate C_N and C_m to be linear with α, so to a first approximation

$$\begin{aligned} C_N &\approx C_{N_\alpha} \alpha \\ C_m &\approx C_{m_\alpha} \alpha \end{aligned} \tag{3.15}$$

The Barrowman method[16] uses the coefficient derivatives to determine the CP position using Equation (3.12). However, there are some significant nonlinearities in the variation of C_N as a function of α. These will be accounted for by holding the approximation of Equation (3.15) exact and letting C_{N_α} and C_{m_α} be a function of α.

3.2.2. Normal Forces and Pitching Moments

Barrowmans method[16] for determining the total normal force coefficient derivative C_N , the pitch moment coefficient derivative C_m and the CP location at subsonic speeds first splits the rocket into simple separate components, then calculates the CP location and C_{N_α} for each component separately and then combines these to get the desired coefficients and CP location.

The general assumptions made by the derivation are:

1. Nearly zero is the angle of attack.
2. The flow is steady and rotational.
3. The vehicle's body is rigid.
4. The tip of the nose is a sharp point.
5. The vehicle's body is axially symmetrical and slim.

The steady state running normal load in the assumed bodies is, for subsonic flow: The steady state running normal load in the assumed bodies is, for subsonic flow:

$$n(x) = \rho V \frac{\partial}{\partial x} [A(x)w(x)] \tag{3.16}$$

Where $A(x)$ is the cross-sectional area of the body and $w(x)$ is the rigid body downwash,

$$w(x) = V \sin(\alpha) \tag{3.17}$$

By combining Equation (3.16) with Equation (3.17) and replacing in the definition of normal force coefficient, one can integrate along the body's length to obtain,

$$C_N = \frac{2\sin(\alpha)}{A_{\text{ref}}} [A(l_0) - A(0)] \tag{3.18}$$

Where A_{ref} is the maximum cross-sectional area of the rocket.

3.2.2.1 Body Lift: Equation (3.18) neglects body lift. However, in the flight of long, slender rockets, as well as for most rockets at high angles of attack, the lift might be considerable, usually shifting the centre of pressure towards the geometric centre of the rocket, which will affect its stability (or lack of thereof).

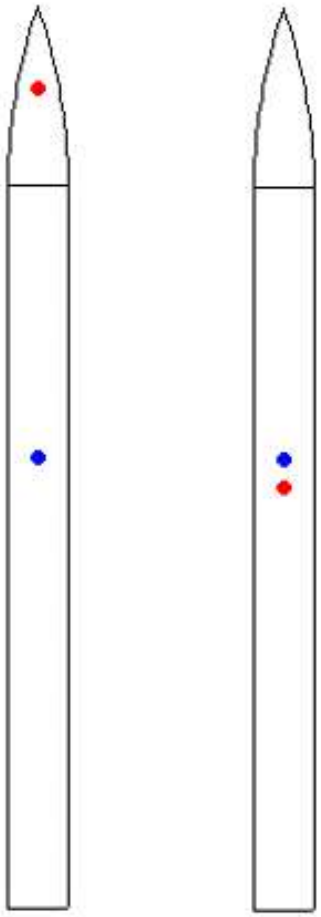

Figure 3.6: Example of effect of body lift on C_p location, showing the C_p at $\alpha = 0^o$ (left) and $\alpha = 90^o$ (right)

To solve the issue, Robert Gallejs[13] suggested adding a correction term in the form of,

$$C_N = K\frac{A_{plan}}{A_{ref}}sin^2(\alpha) \tag{3.19}$$

where $A_{plan} = d.l$ is the planar area of the component, and K is a constant ranging from $K \approx 1.1$ to $K \approx 1.5$, where the lower value is used.

3.2.2.2 Total Normal Force Coefficient The total normal force coefficient produced by each body component can be expressed as the sum of Equation (3.18) and Equation (3.19),

$$C_{N_i} = \frac{2\sin(\alpha_i)\cos(\alpha_i)}{A_{\text{ref}}}\left[A(l_0)_i - A(0)_i\right] + \mathbf{K}\frac{A_{\text{plan},i}}{A_{\text{ref}}}\sin^2(\alpha_i)$$

Where $cos(\alpha_i)$ is added to better match the centre of pressure and normal force coefficient at $\alpha > 45$ .For example, in the case of a solid cylinder at α=90 º

$$C_D = C_{N_{\alpha=90^o}} \frac{A_{ref}}{A_{plan}} = 1.1$$

Which is not the result obtained if one uses the unmodified Extended Barrowman Equations[13].

3.2.3. Roll Dynamics

The fins will cause a roll moment on a rocket if they are canted at an angle $\delta > 0$ with respect to the rocket centerline. Canting the fins will result in a non-zero rolling moment but no corresponding net force, in contrast to the normal force and pitching moment. Therefore the only quantity computed is the roll moment coefficient, defined by

$$C_l = \frac{l}{\frac{1}{2}\rho v_o^2 A_{ref} d} \tag{3.20}$$

where l is the roll moment.

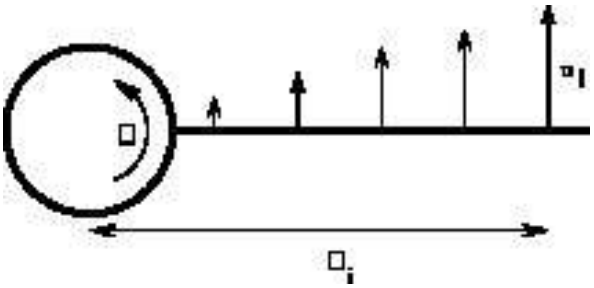

Figure 3.7: Radial velocity at various fin locations. Viewed from the rocket's back.

There are no forces that would result in net yawing moments for rockets with axially symmetrical fin designs. Nonetheless, all six kinds of forces and moments can be generated by a single fin. By splitting the fin into thin, streamwise strips and then integrating across the strips, one can investigate the impact of roll on a fin. A strip i at distance i from the rocket centerline encounters a radial velocity

$$u_i = \omega \xi_i \tag{3.21}$$

where ω is the angular roll velocity, as shown in Figure 3.7. The radial velocity induces an

angle of attack

$$\eta_i = \tan^{-1}\left(\frac{u_i}{v_0}\right) = \tan^{-1}\left(\frac{\omega\xi_i}{v_0}\right) \approx \frac{\omega\xi_i}{v_0} \tag{3.22}$$

to the strip. The approximation $\tan^{-1}\eta \approx \eta$ is valid for $u_i \ll v_0$, that is, when the velocity of the rocket is large compared to the radial velocity. The approximation is reasonable up to angles of $\eta \approx 20^\circ$, above which angle most fins stall, which limits the validity of the equation in any case.

When a fin is canted at an angle δ, the total inclination of the strip to the airflow is

$$\alpha_i = \delta - \eta_i. \tag{3.23}$$

Assuming that the force produced by a strip is directly proportional to the local angle of attack, the force on strip i is

$$F_i = k_i\alpha_i = k_i(\delta - \eta_i) \tag{3.24}$$

for some k_i. The total moment produced by the fin is then

$$l = \sum_i \xi_i F_i = \sum_i \xi_i k_i(\delta - \eta_i) = \sum_i \xi_i k_i \delta - \sum_i \xi_i k_i \eta_i. \tag{3.25}$$

This indicates that the roll effect can be divided into two parts: the opposing moment produced by an uncanted fin ($\delta = 0$) when flying at a roll rate ω, and the roll moment caused by a fin canted at the angle δ when flying at zero roll rate ($\omega = 0$), which is represented by the first term $\sum_i \xi_i k_i \delta$. The roll damping moment and the roll forcing moment are the names given to these two moments, respectively.

3.2.3.0.1 Roll Forcing Coefficient A rocket with fins canted at an angle and traveling at zero roll rate (ω= 0) can be used to calculate the roll forcing coefficient. In this instance, the cant angle only serves as each fin's angle of attack. As a result, the techniques calculated in the preceding section are directly applicable. Because the lift force of a fin originates from the **mean aerodynamic chord**, the roll forcing coefficient of N fins is equal to

$$C_{lf} = \frac{N(y_{MAX} + r_t)(C_{N_\alpha})_1 \delta}{d} \tag{3.26}$$

3.2.3.0.2 Roll Damping Coefficient A rocket with uncanted fins (δ = 0) traveling at a roll rate ω is used to calculate the roll damping coefficient. The damping moment needs to be calculated from the individual streamwise airfoil strips because various parts of the fin

experience different local angles of attack.

At subsonic speeds the force generated by strip i is equal to

$$F_i = C_{N,0}\frac{1}{2}\rho v_0^2 \frac{c_i \Delta\xi_i}{\text{area}}\eta_i. \tag{3.27}$$

Here $C_{N,0}$ is calculated by equation,

$$C_{N_\alpha} = \frac{2\pi}{\beta} \tag{3.28}$$

where, $\beta = \sqrt{1-M^2}$ for $M < 1$. Based on thin airfoil theory of potential flow corrected for compressible flow.

and $c_i\Delta\xi_i$ is the area of the strip. The roll damping moment generated by the strip is then

$$(C_{dl})_i = \frac{F_i \xi_i}{\frac{1}{2}\rho v_0^2 A_{ref} d} = \frac{C_{N,0}}{A_{ref} d}\xi_i c_i \Delta\xi_i \eta_i. \tag{3.29}$$

By applying the approximation (3.22) and summing (integrating) the airfoil strips the total roll damping moment for N fins is obtained as:

$$C_{dl} = N\sum_i (C_{dl})_i = \frac{NC_{N,0}\omega}{A_{ref} d v_0}\sum_i c_i \xi_i^2 \Delta\xi_i. \tag{3.30}$$

The sum term is a constant for a specific fin shape. It can be computed numerically from the strips or analytically for specific shapes. For trapezoidal fins the term can be integrated as

$$\sum_i c_i \xi_i^2 \Delta\xi_i = C_r\left(\frac{C_r + C_t}{2} r_1 s^2 + \frac{C_r + 2C_t}{3} r_1 s^2 + \frac{C_r + 3C_t}{12} s^3\right). \tag{3.31}$$

For elliptical fins

$$\sum_i c_i \xi_i^2 \Delta\xi_i = C_r\left(\frac{\pi}{4} r_1 s^2 + \frac{2}{3} r_1 s^2 + \frac{\pi}{16} s^3\right). \tag{3.32}$$

An equivalent calculation of the roll damping moment at supersonic speeds begins with the supersonic strip lift force equation,

$$F_i = C_{p_i}\frac{1}{2}\rho v_o^2 c_i \Delta y \tag{3.33}$$

where Equation (3.22) is used to determine each strip's angle of inclination. At supersonic

speeds, the roll moment is

$$C_{dl} = \frac{N}{A_{ref} d} \sum_i C_{P_i} c_i \xi_i \Delta\xi_i. \tag{3.34}$$

Since the dependency is non-linear, the sum term depends on both the fin shape and the Mach number. The dependence on the incidence angle η_i is buried inside the local pressure coefficient C_P.

3.3. Control System

To implement precision stability and especially guidance, static stability is not enough. It needs a control system that controls the vehicle's fins in real time based on the position and orientation of the vehicle. A control system is a set of devices or mechanisms that manages, commands, directs, or regulates the behavior of other devices or systems with a feedback mechanism.

Key Components of a Control System include:

1. Controller: The brain of the control system, it processes inputs and determines the necessary actions to achieve the desired output.
2. Sensors: Devices that measure variables (e.g., temperature, pressure, speed, orientation) and provide feedback to the controller.
3. Actuators: Devices that execute the controller's commands to influence the system (e.g., motors, valves).
4. Set-point: The desired value or state that the control system aims to maintain.
5. Feedback Loop: The process of continuously measuring the output, comparing it to the set-point, and adjusting inputs accordingly.
6. Control Algorithm: Mathematical and logical rules that the controller uses to determine the appropriate control action. There are different control methods like PID control, LQR, MPC adaptive control, or state-space control.

3.4. PID

PID control is one of the most widely used control algorithms in industrial and automation systems due to its simplicity and effectiveness. It combines three types of control ac-

tions—proportional, integral, and derivative—to provide a control signal that corrects errors between a desired set-point and the actual process variable.

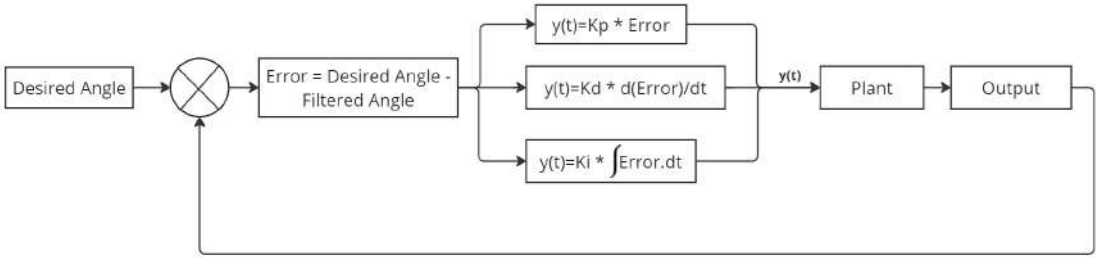

Figure 3.8: PID controller with feedback loop

- **Control Error ($e(t)$)**: The difference between the desired set-point $r(t)$ and the measured process variable $y(t)$:

$$e(t) = r(t) - y(t) \tag{3.35}$$

- **Control Output ($u(t)$)**: The signal sent to the actuator to correct the error. In PID control, $u(t)$ is computed as the sum of three terms: proportional, integral, and derivative.

1. Proportional Control (P): The proportional term produces an output that is proportional to the current error value. It is the simplest form of control, where the control action is directly proportional to the error.

$$u_P(t) = K_P e(t) \tag{3.36}$$

   Where K_P is the proportional gain, which determines the reaction to the current error.

2. Integral Control (I): The integral term is concerned with the accumulation of past errors. If the error has been present for a while, the integral term increases the control output, which helps eliminate residual steady-state errors.

$$u_I(t) = K_I \int_0^t e(\tau) d\tau \tag{3.37}$$

   Where K_I is the integral gain, which determines the reaction to the sum of past errors.

3. Derivative Control (D): The derivative term predicts future error based on its rate of change. It provides a control output that is proportional to the rate of change of the error, helping to reduce overshoot and improve stability.

$$u_D(t) = K_D \frac{de(t)}{dt} \tag{3.38}$$

Where K_D is the derivative gain, which determines the reaction to the rate of change of the error.

PID Control Equation

The PID control law is the sum of the proportional, integral, and derivative terms:

$$u(t) = K_P e(t) + K_I \int_0^t e(\tau) d\tau + K_D \frac{de(t)}{dt} \tag{3.39}$$

Alternatively, it can be written as:

$$u(t) = K_P \left[e(t) + \frac{1}{T_I} \int_0^t e(\tau) d\tau + T_D \frac{de(t)}{dt} \right] \tag{3.40}$$

where $T_I = \frac{1}{K_I}$ is the integral time and $T_D = K_D$ is the derivative time.

3.5. Kalman Filter

The Kalman Filter is a powerful mathematical tool used in control systems, signal processing, and navigation for estimating the state of a dynamic system from a series of noisy measurements. Named after Rudolf E. Kalman, who developed the filter in the 1960s, it provides optimal estimates by minimizing the mean square error. Its applications range from aerospace and robotics to finance and economics, making it a foundation in modern control theory.

In rocket trajectory estimation, the Kalman Filter can be used to combine measurements from sensors (such as gyroscopes, accelerometers, and GPS) to accurately estimate the rocket's position, velocity, and orientation. The state vector might include position coordinates, velocity components, and attitude angles. The filter recursively updates these estimates based on sensor data, accounting for noise and disturbances, ensuring accurate tracking of the rocket's trajectory throughout its flight.

KF algorithm differs from the conventional method of timing prediction. It can estimate the

system's state via a set of incomplete observations (i.e. missing time points in time-series data) or noisy observations (measurement error). The KF is a fast recursive filter model. It takes up small memory and only needs to retain data for system's state at a time, rather than a long period of time. The actual measured data are used to correct the estimated results[17].

It operates in two main steps: prediction and update. In the prediction step, the algorithm estimates the current state The Kalman Filter operates in two main steps: prediction and update. In the prediction step, it estimates the current state $\hat{x}_{k|k-1}$ and error covariance $P_{k|k-1}$ based on the previous state estimate, control inputs, and the state transition matrix F_k. This step projects forward the state estimate given the dynamics of the system and any control inputs.

$$\hat{x}_{k|k-1} = F_k \hat{x}_{k-1|k-1} + B_k u_k \tag{3.41}$$

$$P_{k|k-1} = F_k P_{k-1|k-1} F_k^T + Q_k \tag{3.42}$$

where $\hat{x}_{k-1|k-1}$ is the previous state estimate at time $k-1$, B_k is the control input matrix, u_k is the control input at time k, $P_{k-1|k-1}$ is the error covariance matrix of the state estimate at time $k-1$, F_k^T is the transpose of F_k, and Q_k is the process noise covariance matrix.

In the update step, the Kalman Filter incorporates the latest measurement (z_k) to refine the state estimate and its associated uncertainty. The Kalman Gain (K_k) determines how much weight to give to the measurement relative to the predicted state estimate, adjusting the state estimate ($\hat{x}_{k|k}$) and error covariance ($P_{k|k}$) accordingly. [18].

$$K_k = P_{k|k-1} H_k^T (H_k P_{k|k-1} H_k^T + R_k)^{-1} \tag{3.43}$$

$$\hat{x}_{k|k} = \hat{x}_{k|k-1} + K_k(z_k - H_k \hat{x}_{k|k-1}) \tag{3.44}$$

$$P_{k|k} = (I - K_k H_k) P_{k|k-1} \tag{3.45}$$

where H_k is the measurement matrix which maps the state space into the measurement space, H_k^T is the transpose of H_k, R_k is the measurement noise covariance matrix, z_k is the measurement at time k, and I is the identity matrix.

3.6. Computational Fluid Dynamics (CFD)

Computational Fluid Dynamics (CFD) is a tool built on the principle of fluid dynamics that utilizes discretization techniques and solve the problem accordingly in each discrete points. At the beginning of time, to see the behaviour of air flow around body wind tunnels were

used but as the time progressed CFD gradually penetrated into the engineering process as a complement to various categories of testing. CFD from being a tool to add depth to information, became a primary source for engineering practice in case of vehicles with narrow flight envelope as missiles or model rockets [8].

The CFD can be used for the conceptual and preliminary design of the rocket. For the final design it is recommended to validate the results with wind tunnel.This strategy of integration is an emerging trend and must be strongly encouraged and developed for the maturation of the CFD approach [9]. The fins of rocket, whether active or passive, plays a massive role in maintaining stability. CFD can be used to explore various configuration of the fins and how they correlate with the interested parameter as the drag & lifting forces.

4. METHODOLOGY

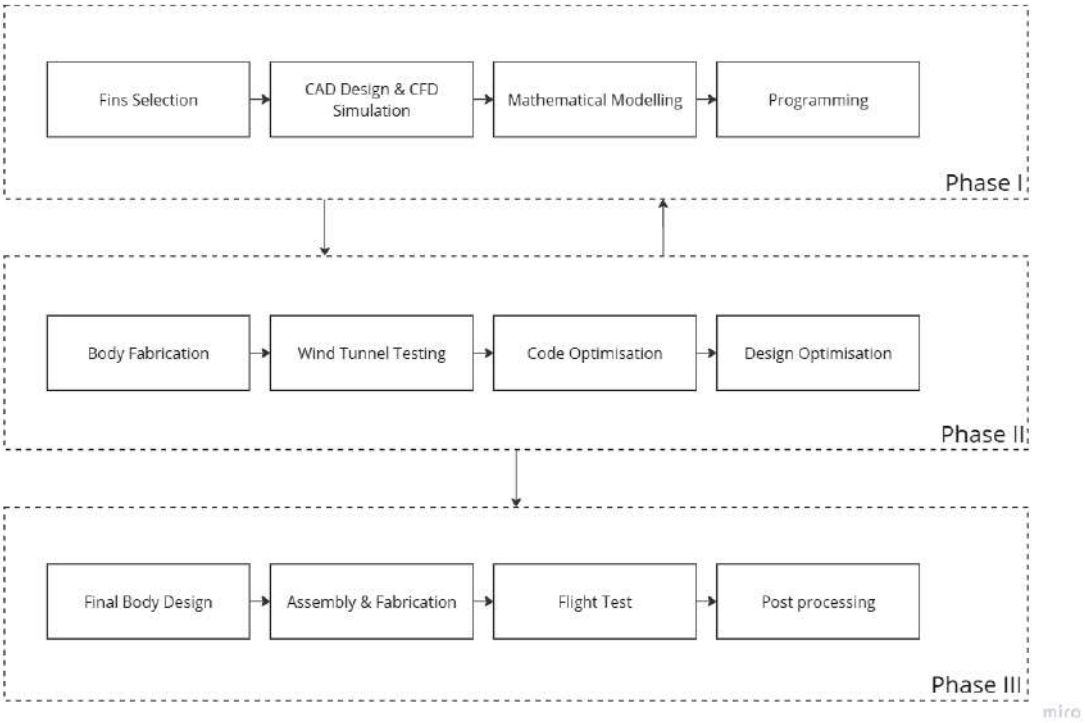

Figure 4.1: Methodology

4.1. Control system

Designing a control system involves several steps:

1. Modeling the System: Creating a mathematical representation of the system's dynamics.
2. Choosing Control Strategy: Selecting between different control methods like PID control, adaptive control, or state-space control.
3. Implementing Controllers: Design and programming of the controllers based on the chosen strategy.
4. Simulation and Testing: Using simulations to predict system behavior and conducting real-world tests to validate the design.

5. Optimization and Tuning: Adjusting parameters to improve performance and efficiency.

Figure 4.2: Control system

4.2. Mathematical Modeling

4.2.1. AeroVECTOR

AeroVECTOR, model rocket simulator designed for active control system development and tuning is used for the mathematical modeling of our active fins-controlled rocket to analyze its stability and simulate guidance. It allows for the tuning of controllers used in model rockets by integrating the Three Degree of Freedom Equations of Motion. The software calculates the rocket's 3DoF equations of motion and applies the trapezoidal rule to the result. With a few adjustments, Open Rocket's Extended Barrowman Equations are used to compute the aerodynamic coefficients. Diederich's Semi-Empirical Method and interpolated wind tunnel data are used to calculate the fins' forces in order to precisely model the behavior for each aspect ratio and angle of attack. Additionally, the program permits fins to be removed from the body.

4.2.1.1 Input parameters: Following Input parameters were defined in the simulation where,

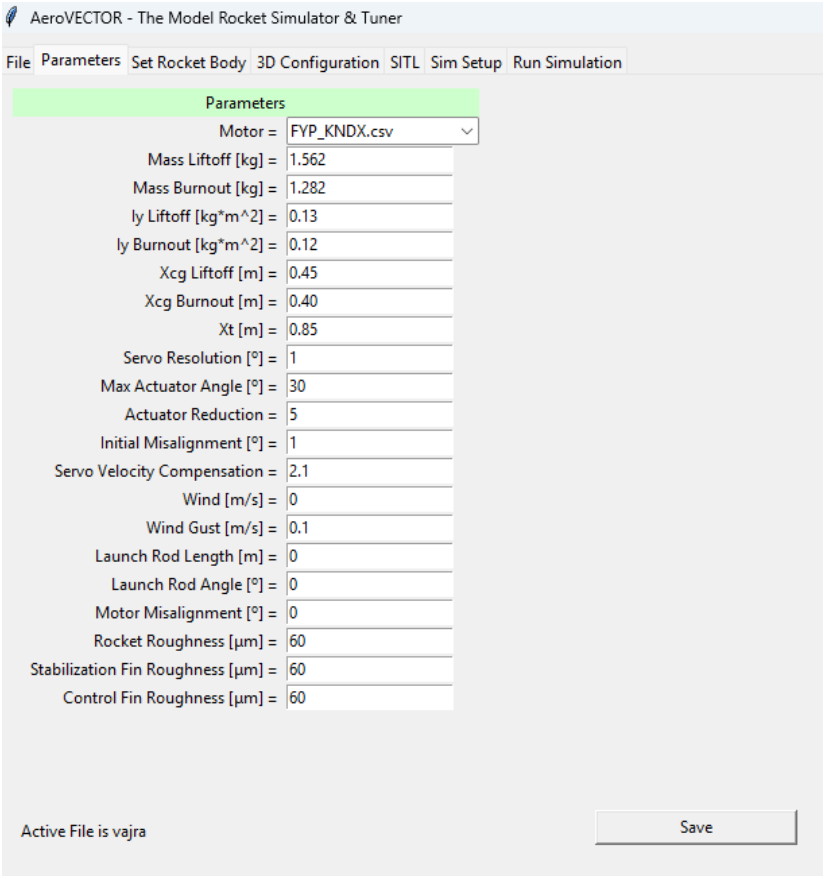

Figure 4.3: AeroVECTOR parameters

- Iy Liftoff/Burnout are the pitching moment of inertia at the time of launch and after the complete burnout of rocket's motor.
- Xcg Liftoff/Burnout are the position of the Center of Gravity at the time of launch and after the complete burnout of rocket's motor.
- Xt is the position of the TVC mount. In case fins, the program itself calculates the force application point[4].
- All distances are measured from the tip of the nose cone[4].
- The Servo Resolution is the minimum angle it can rotate[4].
- The Max Actuator Angle is the maximum angle the actuator can move (either the TVC mount or the fin)[4].
- The Actuator Reduction is the gear ratio between the servo and the actuator[4].
  - The code multiplies the output of the controller times the Actuator Reduction, and then sends that output to the SERVO (not the mount)[4]. Remember that you

have to multiply the output of the controller times the Actuator Reduction in your flight computer![4]

- The Initial Misalignment only modifies the initial angle of the TVC mount or Active Fin[4].
- The Servo Velocity Compensation slows down the servo according to the load[4],
- The wind is positive from right to left, and the gusts follow a Gaussian distribution[4].
- The effective launch rod length is the length at which the rocket can pitch somewhat freely[4].
- Angle of the launch rod[4].
- The Motor Misalignment sets the motor at an angle (mainly for active fin control)[4].
- The roughness applies to all the components of the body and fins; therefore, a little tuning might be required to get the performances right[4].

4.2.1.2 Setting Rocket Body:

Here, the rocket body was designed by inserting points.

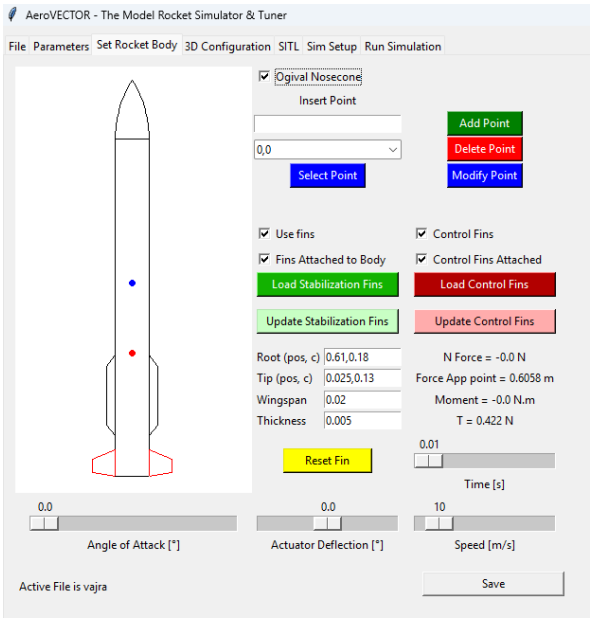

Figure 4.4: Setting rocket body

4.2.1.3 Simulation Setup:

This window was used to setup the simulation.

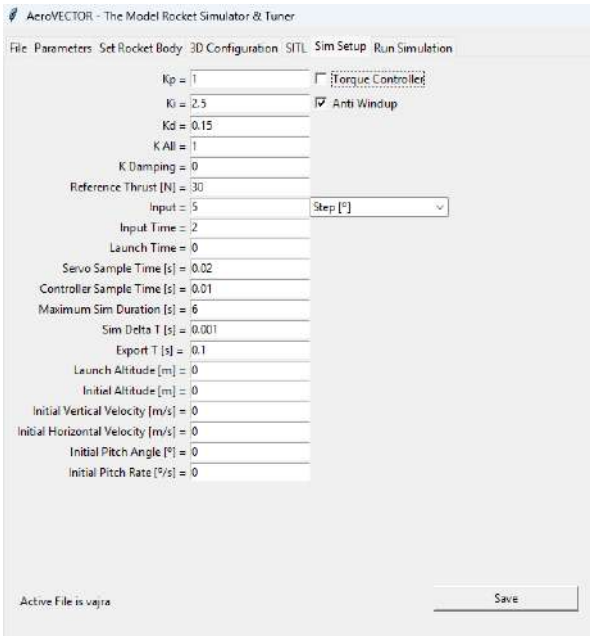

Figure 4.5: AeroVECTOR simulation setup

where,

- Kp, Ki, and Kd are the gain values of PID Controller[4].
- K All scales the error before sending it to the PID[4].
- K Damping feeds the gyro back at the output of the PID and acts as damping[4].
  - To disable the controller, one must set K All and K Damping to zero[4].
  - In case the Control Fins are ahead of the CG, the controller multiplies K All and K Damping by -1[4].
- Reference Thrust is the Reference Thrust of the Torque Controller, more info in the `control.py` file[4].
- Input is the input to the rocket, be it a Step (deg) or a Ramp (deg/s)[4].
  - If the selected input is Up, then this entry is bypassed[4].
- Input Time is the instant at which the input is changed from 0 to the selected one[4].
- Launch Time is the instant at which the motor is ignited[4].
- Servo Sample Time and Program Sample Time are self-explanatory, note they are in seconds and not Hz[4].

- Maximum Sim Duration specifies the maximum duration of the simulation[4].
  - The simulation will stop if the rocket tumbles more than 2 times, hits the ground, or coasts for more than 10 burnout times[4].
- Sim Delta T is the sample time of the simulation; one can increase it to hasten it[4].
  - Since the Software-in-the-Loop simulation runs in real time, this setting does not affect it[4].
- Export T is the sample time of the data exports, i.e., the time between exported data points[4].
- Launch altitude is the height above sea level of the launchpad[4].
- The next entries deal with the initial state of the rocket, useful for second stages or landings (landing aerodynamics are not well modeled; please do not rely exclusively on them)[4].

4.2.1.4 Simulation Results: This is where the simulation is visualized and the output data is plotted and analyzed.

Figure 4.6: Rocket Orientation at t = 1.5 seconds (Setpoint = 0 degree)

Figure 4.7: Rocket Orientation at t = 4 seconds (Setpoint = 5 degree)

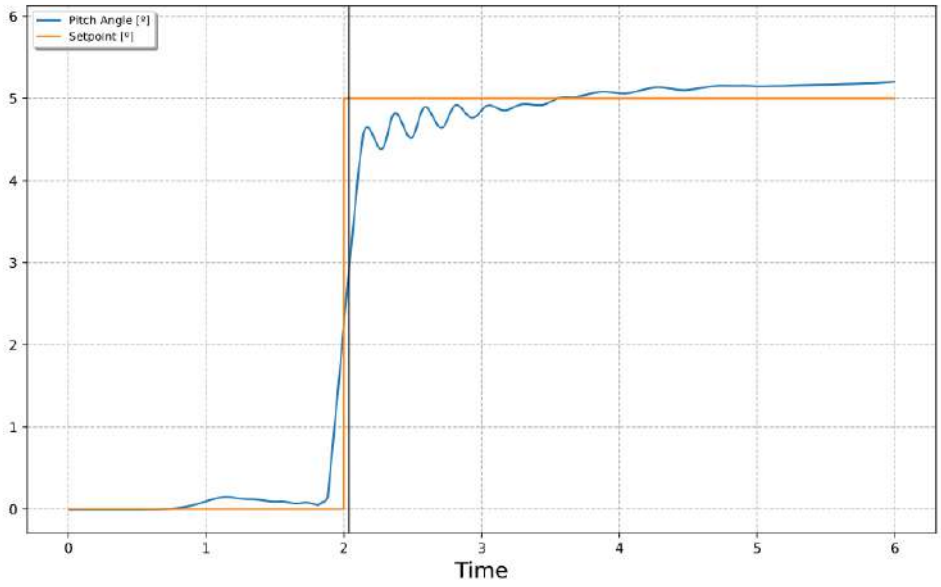

Figure 4.8: Input vs output pitch angle

The multiple simulations were run to perfectly tune the model and simulate flight behavior as desired.

4.2.2. MATLAB/Simulink Model

The need of our self developed simulink model raised with the limitation of Aerovector as a software to tune the roll of the rockets. The Aerovector was not designed to take the roll characteristics into action. Thats why, the self made, physics based mathematical model is developed.

The following blocks were used to model the rocket dynamics:

4.2.2.1 Simple Variable Mass 6DOF (Euler Angles): The Simple Variable Mass 6DOF (Euler Angles) block considers the rotation of a body-fixed coordinate frame (Xb, Yb, Zb) about a flat Earth reference frame (Xe, Ye, Ze).

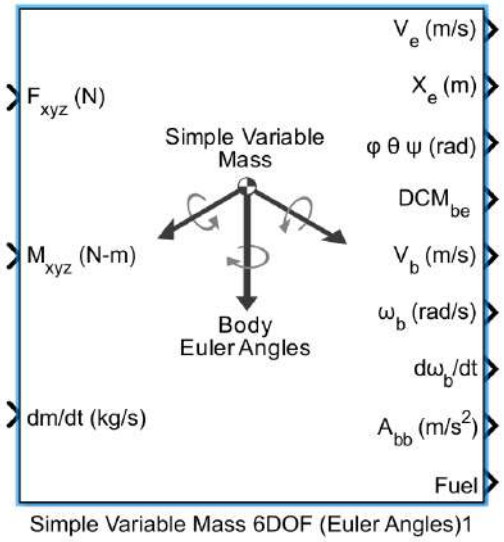

Figure 4.9: 6 DOF simple variable mass (Euler Angle)

The origin of the body-fixed coordinate frame is the center of gravity of the body, and the body is assumed to be rigid, an assumption that eliminates the need to consider the forces acting between individual elements of mass. The flat Earth reference frame is considered inertial, an excellent approximation that allows the forces due to the Earth's motion relative to the fixed stars to be neglected. This blocks takes the Forces and Moments as input and gives the body's attitude as output, which is fed back to the PID controller.

4.2.2.2 PID Controller Block: This block represents the control algorithm of our control system. The PID Controller block implements a PID controller (PID, PI, PD, P only, or I only). The block is identical to the Discrete PID Controller block with the Time domain parameter set to Continuous-time.

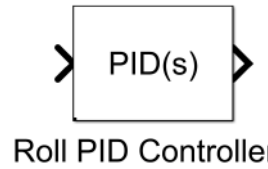

Figure 4.10: PID controller

The block output is a weighted sum of the input signal, the integral of the input signal, and the derivative of the input signal. The weights are the proportional, integral, and derivative gain parameters. A first-order pole filters the derivative action. This block implements

continuous- and discrete-time PID control algorithms and includes advanced features such as anti-windup, external reset, and signal tracking.

4.2.2.3 Band Limited White Noise: The Band-Limited White Noise block generates normally distributed random numbers that are suitable for use in continuous or hybrid systems. This block was used to simulate the sensor noise.

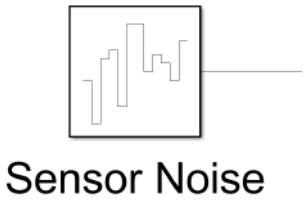

Figure 4.11: Sensor noise

The output of this block was connected to the roll angle of the body which is fed to the PID controller.

4.2.2.4 1st Order Transfer Function (Actuator) This block was used to model the actuator dynamic, which is servo motor in our case.

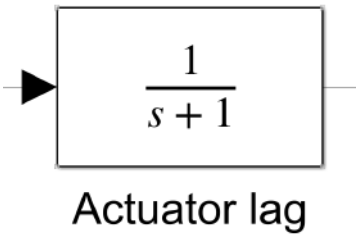

Figure 4.12: 1st order transfer function

First order Transfer Function was used to model the lag response of the Actuator.

4.2.2.5 1D-Lookup Table: This block is used to index the lift coefficient(C_l) and drag coefficient(C_D) based on angle of attack(α), which is the output of PID controller and speed(u), which is the output of 6DOF Block.

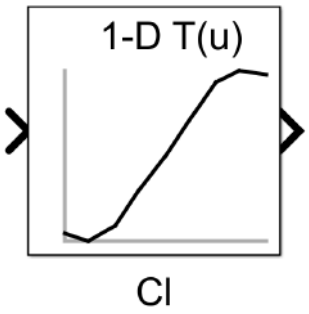

Figure 4.13: 1D lookup table

This table is used to perform a 1-dimensional interpolated table lookup, including index searches. The table is a sampled representation of a function in 1 variables. Breakpoint sets relate the input values to positions in the table.

4.2.2.6 Transport Delay: This block is used to apply the specified delay to the input signal. Hence, it was used to model the sensor's latency.

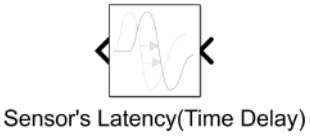

Figure 4.14: Transport Delay

4.2.2.7 From workspace block: This block is used to import the thrust curve data. The result of the performed static test was imported in csv format as thrust input to the 6DOF block.

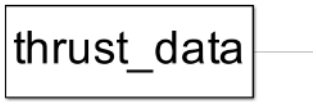

Figure 4.15: From workspace

4.2.2.8 Rate Limiter: This block is used to limit the maximum rate of rise and fall of signal. In out case, it is used to model the maximum servo speed.

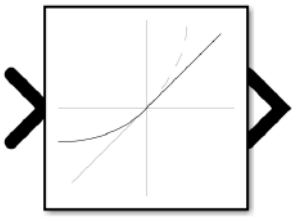

Figure 4.16: Rate limiter

4.2.2.9 Zero-order Hold This block is used to hold the signal for certain period to simulate real time latency of the processor.

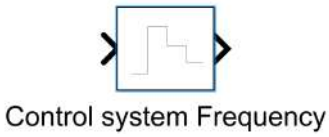

Figure 4.17: Zero order hold

4.2.2.10 Detailed Mathematical Model The final mathematical model looks like this:

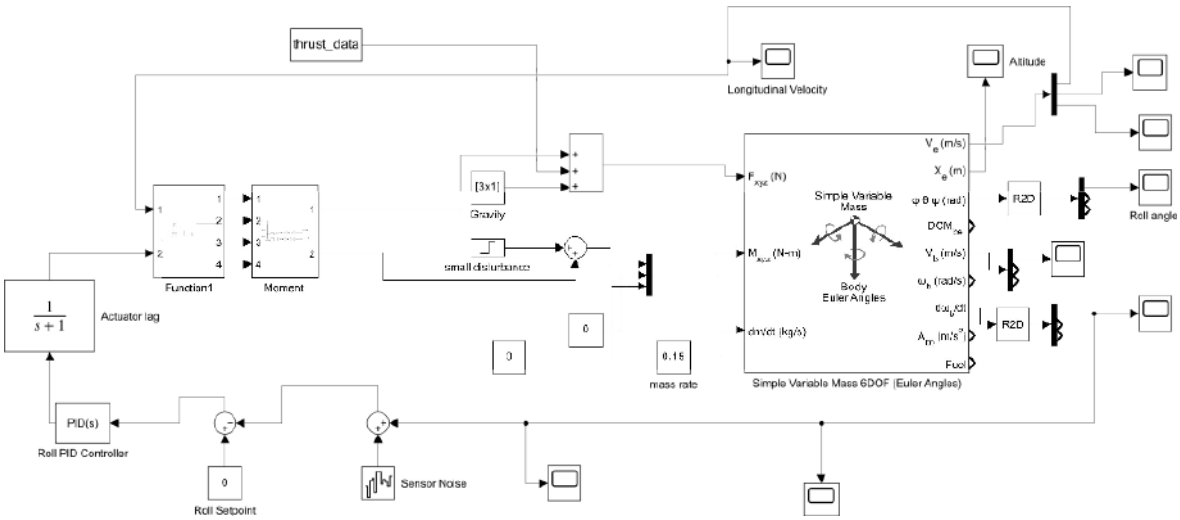

Figure 4.18: Detailed mathematical model

4.2.3. Control system Algorithm

The following block diagram represents the algorithm of our control system.

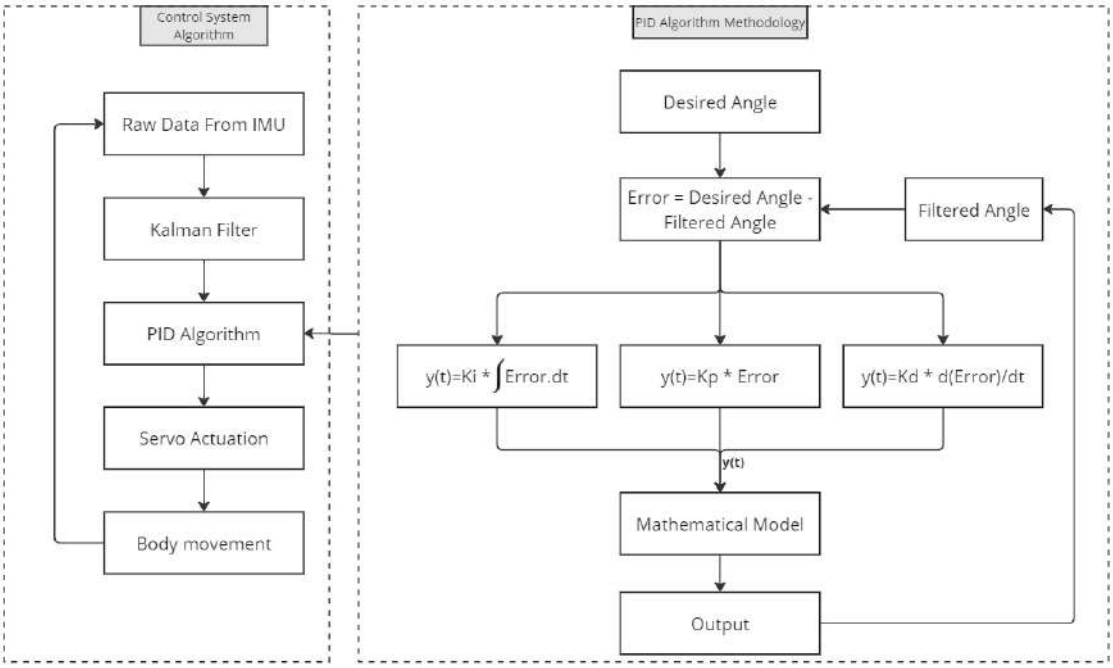

Figure 4.19: Control system programming algorithm

This diagram outlines the control system and PID algorithm methodology for a system that uses IMU data to achieve precise angle control. The control system algorithm starts by collecting raw data from the IMU, which is then filtered using a Kalman filter to reduce noise and provide more accurate data. The filtered data are fed into a PID algorithm, which determines the necessary corrections and sends signals to the servo actuators. These actuators adjust the movement of the body to the desired angle.

The methodology of the PID algorithm begins with the definition of a desired angle. The system calculates the error as the difference between the desired angle and the filtered angle from the IMU data. The proportional component of the PID algorithm multiplies this error by a proportional gain. The integral component takes the integral of the error over time and multiplies it by an integral gain. The derivative component takes the derivative of the error over time and multiplies it by a derivative gain. These components are combined to produce the control output $y(t)$. This output is then used to adjust the system, ensuring that it accurately achieves the desired angle. In summary, the system processes IMU data with a Kalman filter, computes adjustments with a PID algorithm, and uses servo actuation to correct body movement, maintaining a specified angle accurately.

4.3. Flight Computer Development

4.3.1. Schematic Representation

The flight test will be conducted for two different rockets that have different flight computers of each as shown in table 4.1. The following block diagram represents the different flight computers developed for different rockets:

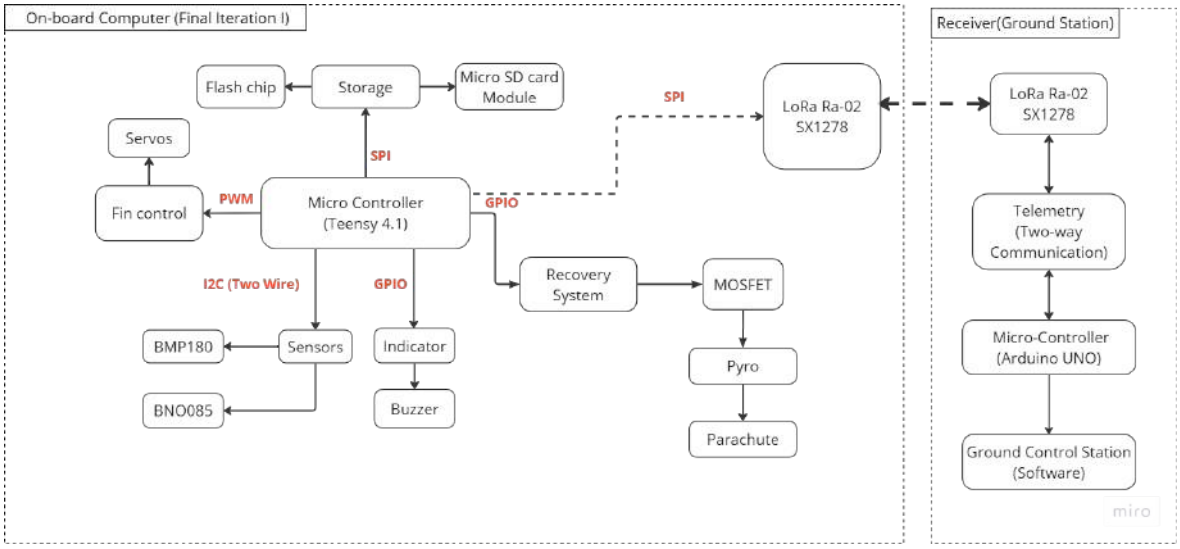

Figure 4.20: Flight computer schematic iteration I

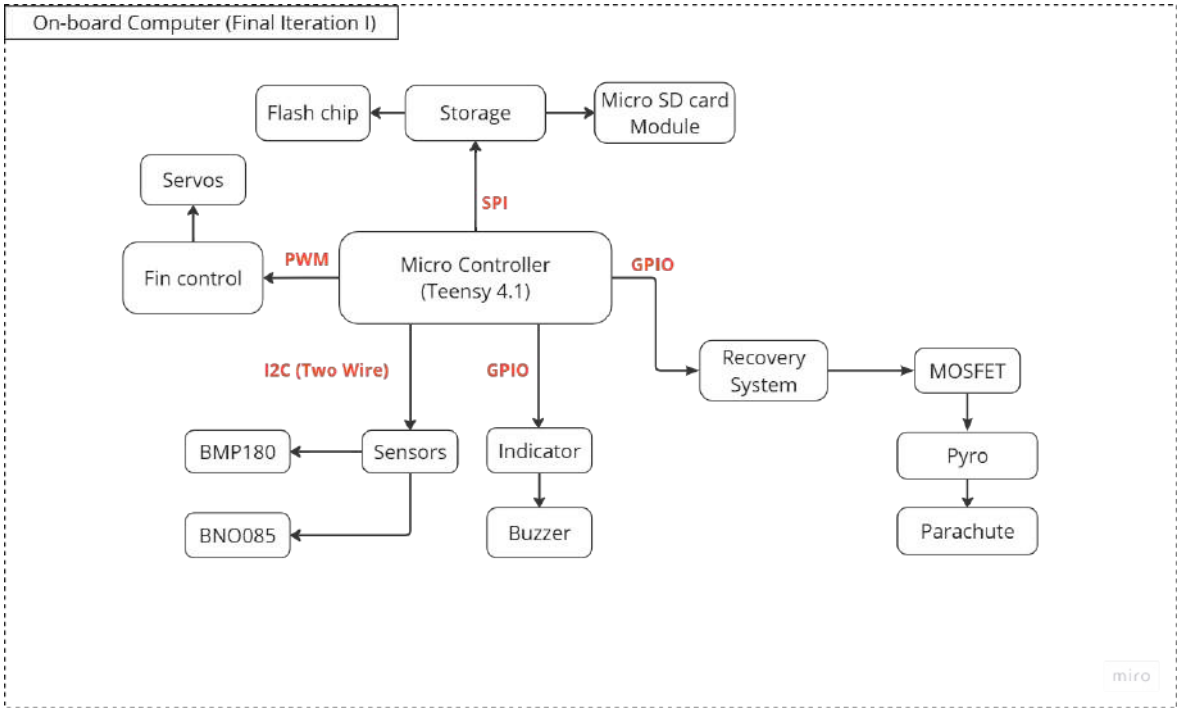

Figure 4.21: Flight computer schematic iteration II

Table 4.1: Flight Computer 1 V/s Flight Computer 2

Flight Computer 1	**Flight Computer 2**
Teensy 4.1	Esp32
Internal Memory	SD Card Module
BN0085	BNO085/MPU6050
BMS-127WV+	BMS-127WV+
BMP180	BMP180
Buck-Boost	Buck-Boost
Lo-Ra Module	—

4.3.2. Programming Algorithm

The following block diagram represents different flight computer programming algorithms to be developed in different phases of our project:

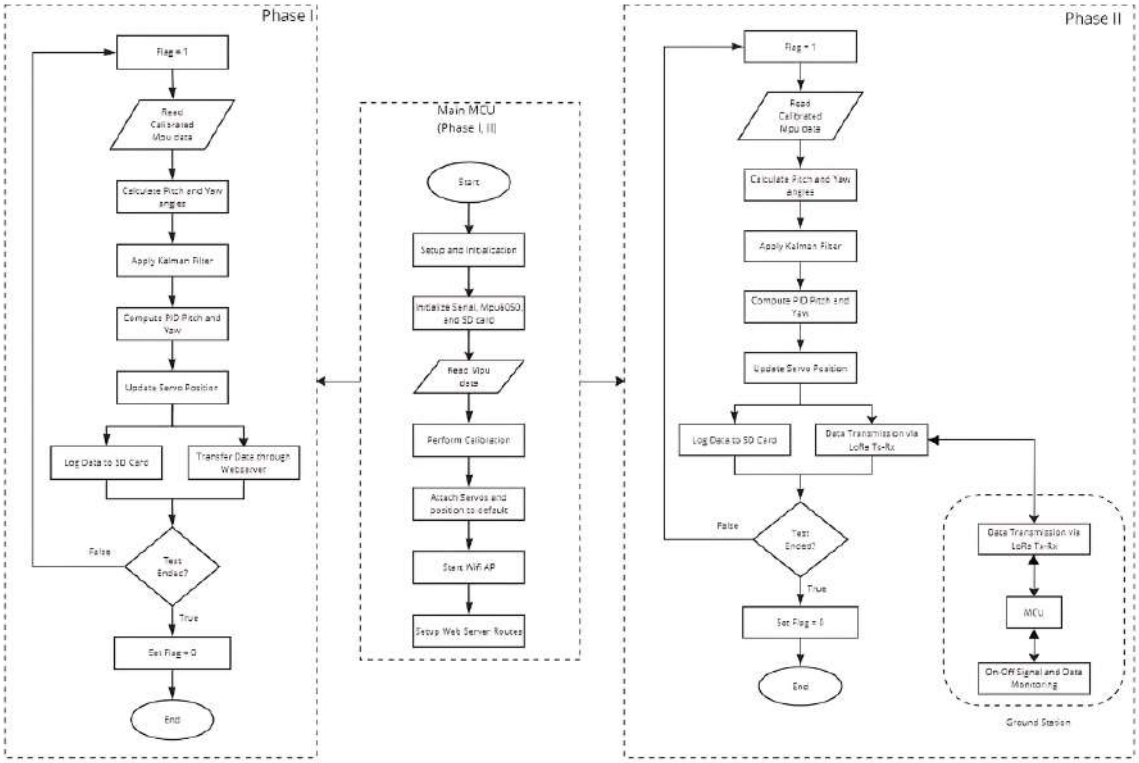

Figure 4.22: Main programming algorithm

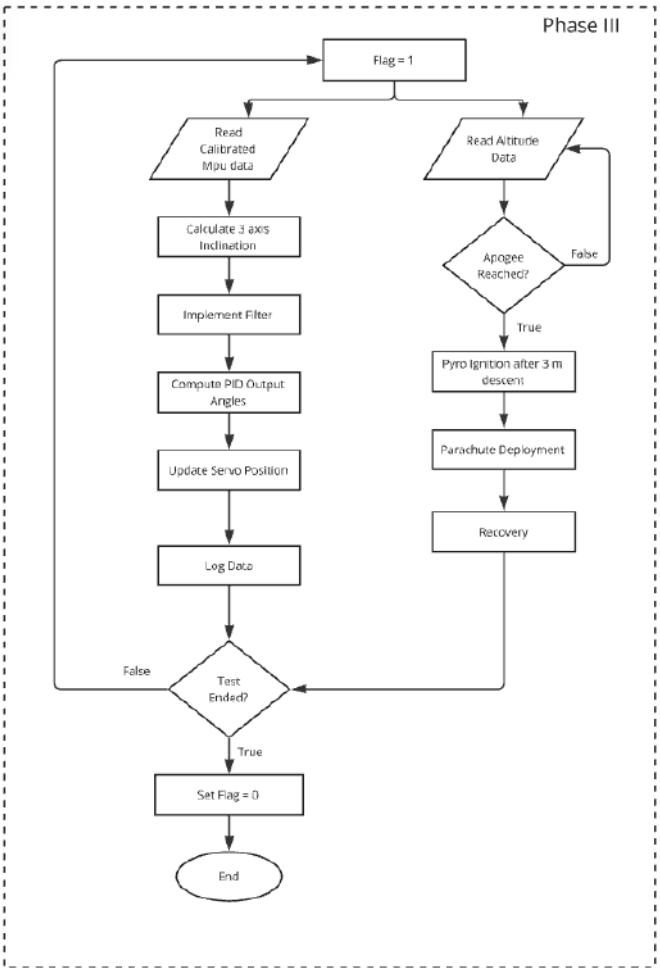

Figure 4.23: Final main programming algorithm

4.3.3. PCB Designing and Fabrication

PCB is the most crucial part of our project as we will be developing multiple hardware components in our avionics system. Before designing the PCB, the circuit was checked and verified using breadboard and matrix board. After verification, the PCB designing was started. For schematic and PCB editing, KiCad software was used and the traces were given suitable width based on their functionality. For fabrication, the PCB design was printed in a glossy paper using printing ink. The ink was then transferred on a cleaned copper board using acetone. After this etching process was carried out. The etching is done by putting the copper board on the solution of HCl and Hydrogen Peroxide in the ratio of 1:3. In 5 minutes, the PCB was ready. Our PCB was fully operational after the drilling and soldering tasks.

The PCB is a crucial part of our project, as it integrates multiple hardware components in our avionics system. Before designing the PCB, we checked and verified the circuit using breadboards and matrix boards. Once verified, we proceeded to PCB designing using KiCad

software for schematic and PCB editing. The traces were assigned suitable widths based on their functionality.

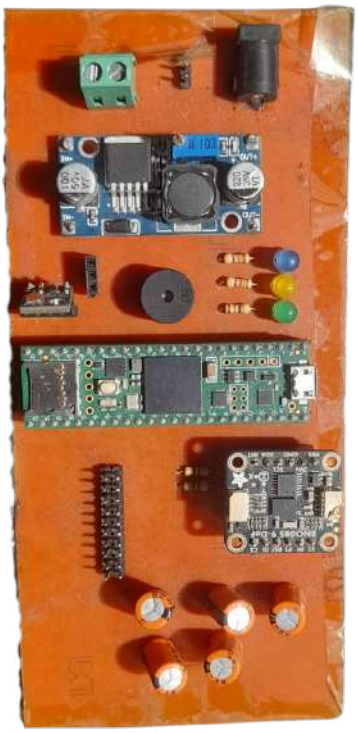

Figure 4.24: Teensy 4.1 based

Figure 4.25: ESP 32 based

Figure 4.26: Avionics bay

4.4. Vehicle Development

4.4.1. Body Fabrication

The fuselage was made using glass fiber composite in the composite lab. The fins, mechanical linkages, and nose cone have all been 3D printed using PLA+ material because of its complexity to meet the design requirements.
450 GSM Fiberglass composites was chosen for the fabrication of rocket body. The mold for the body fabrication was 75mm PVC pipe. A layer of printing paper and a outer layer of cello tape was winded around the pipe for the easiness of mold release after the composite gets settled.

Figure 4.27: Design and fabrication of phase I

Figure 4.28: CAD design of phase II

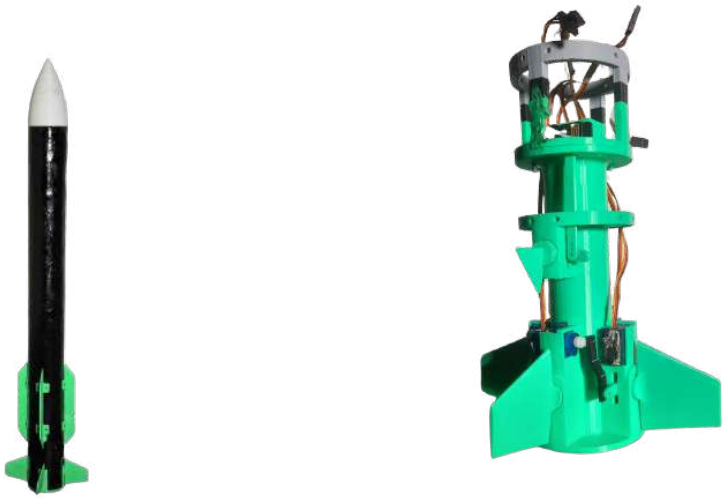

Figure 4.29: Fabrication of phase II

4.4.2. Propulsion System

Propellant Test

A total of three different propellant formulations were tested:

- **KNSU Propellant**
- **Black Powder Propellant**
- **Epoxy-Based Composite Propellant**

Among these propellant KNSU propellant was chosen as the propellant for flight test because of its good characteristics of burn rate, less impact on the composite motor and ease of preparation.

Figure 4.30: Propellant grain of KNDX propellant

Figure 4.31: Motor for black powder propellant

Figure 4.32: Fragments of motor after test

Figure 4.33: Burnt motor after test

Static Thrust Measurement

The static thrust is measured in a Thrust Stand. Loadcell is the sensor used to measure thrust in Newton. The signal from loadcell is amplified using an amplifier HX711 and the data is processed through a Arduino Nano microcontroller. Using this thrust curve, we can analyse and obtain the required fuel composition to achieve desired burn time.

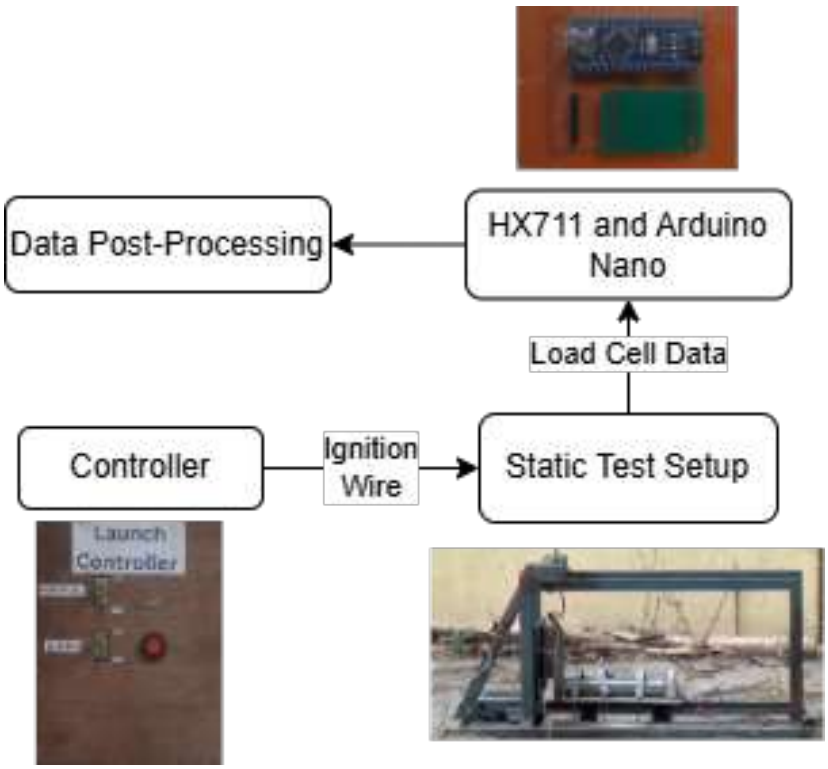

Figure 4.34: Schematic of static thrust test

Ignition System

The rocket ignition systems uses nichrome wire and gunpowder to initiate the motor. A container of gunpowder is positioned above the motor and facing its grain structure. When an electric current passes through the nichrome wire, it heats up, igniting the gunpowder. This ignition triggers a pressure increase within the container, causing the diaphragm to release. This ignition technique ensures simultaneous contact between the ignited gunpowder and the entire length of the fuel grain, promoting a lateral burn and effectively increasing the booster's burn rate. As a result, the rocket experiences enhanced thrust performance during flight.

Motor Casing

The motor dimensions is determined by using simulation software like Openmotor to obtain the desired output. The casing is made from light weight and heat resistant material using glass fiber. The rocket motor is also made up of 450 GSM Fiberglass composite. The mold for the motor was a 32mm pipe. A layer of printing paper and a outer layer of cello tape was winded around the pipe for the easiness of mold release after the composites get set.

Figure 4.35: Composite rocket motor

Nozzle

Various nozzle materials were tested for the rocket motor:

- **Initial Testing with PVC Rocket Motor**

  - Nozzle: Made using a PVC bush with M-seal for the convergent and divergent sections.
  - Purpose: Used for testing gunpowder propellant.

- **Nozzle Variants Tested**
  - **Sheet Metal Nozzle**: The flow did not choke properly, resulting in insufficient thrust.
  - **Mud Nozzle**: Erosion problem.
  - **Composite Nozzle**: Erosion problem.
  - **Graphite Nozzle**: Successfully tested and chosen for flight tests.

Figure 4.36: Mold for composite nozzle

Figure 4.37: Composite nozzle

Figure 4.38: Bush nozzle with Mseal as convergent and divergent Section

Figure 4.39: Sheet metal nozzle

The graphite nozzle may have some problem of irrosion, to encounter this silicone grease, which is a flame resistant lubricant was used. The nozzle design is done using Openmotor, nozzle equations and verified in Ansys. It was manufactured using lathe.

Figure 4.40: Graphite nozzle

4.4.3. Nose Cone and Fins

The nose cone and fins of the body were fabricated using 3D printer. The 3D printing technique was chosen due to the complexity of structure and difficulties in manufacturing.

Figure 4.41: Motor for black powder propellant

Figure 4.42: Fragments of motor after test

4.4.4. Recovery System

The recovery system consists of a parachute, shock cord and canister. Black powder is filled inside the canister. We are using pyro ejection technique for the recovery of the rocket. It uses an ejection charge, in our case it is the black powder to deploy parachute that slows the rocket's descent and allows for a safe landing.

4.4.5. Servo Housing and Linkages

Two different servo housing was designed for different test body. SG90 servos is used in one housing and BMS-147WV+ is used in another. The design of the servo housing was influenced by the size of rocket motor and the body tube as it should fit right in between the rocket motor. The housing and linkages was 3D printed using PLA+.
The servo housing and linkage mechanism for the fins is as shown in Fig . A total of five servos is used in the rocket body, four for the pitch and yaw moment and one for the roll moment. The servo is placed around the rocket motor. The servos is attached to the fins through the linkage mechanism. This housing is attached to the body frame by using bearings.

Figure 4.43: Servo housing and linkages

4.5. Stability Analysis

The rocket's stability needs to be ensured before commencing any other phases of the project. We are making a fin controlled rocket which mainly handles the dynamic stability while

obviously contributing to the static stability along with canard. The stability analysis shows the control effectiveness of the fins in achieving the stability.

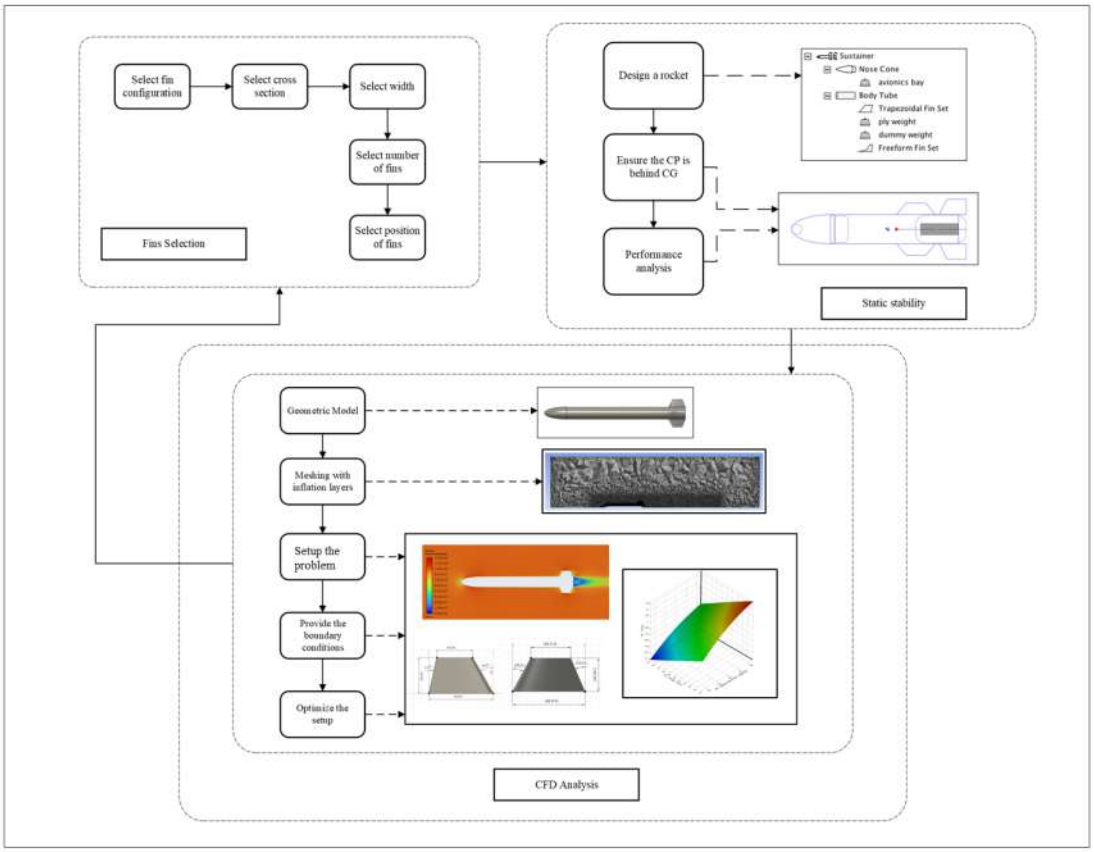

Figure 4.44: Stability Analysis

4.5.1. Selection of fins

The key geometrical parameters that define the fins include airfoil cross-section, tip chord ratio, cant angle, sweep angle, effective aspect ratio, and width. The design process began with a baseline four-fin configuration, derived from historical data. Given that the rocket's maximum velocity is approximately Mach 0.3, with a Reynolds number of 5.6×10, an initial aerodynamic analysis was conducted using XFLR5. This low-fidelity tool, based on the Vortex Lattice Method (VLM), was employed to estimate lift and drag forces. However, it is known that XFLR5 tends to underestimate drag, making it useful primarily for preliminary assessments.

For the airfoil selection, NACA 0015 was chosen based on a balance between structural integrity and aerodynamic performance. While NACA 0012 exhibits a steeper Cl vs curve, the increased thickness of NACA 0015 provides additional structural strength, making it a

more suitable choice. Regarding the fin shape, various configurations were analyzed, and the trapezoidal fin outperformed other designs in terms of aerodynamic efficiency and structural feasibility.

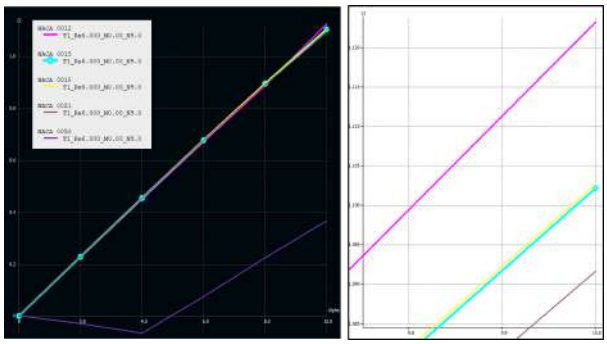

Figure 4.45: Airfoil selection and closeup

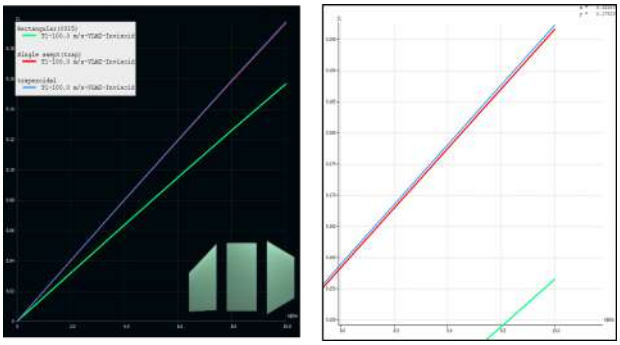

Figure 4.46: Shape selection and closeup

4.6. Fins Configuration

Initially, plus-configuration of fins was chosen for the wind tunnel test. This configuration was a bit ineffective to provide control authority because only two fins were used for the pitch input. Hence, X-configuration of fins was then chosen where all four fins could be used to induce the pitch moment.

For the control of roll moment, a tab from one of the static fins was used. This showed ineffective control authority over the roll moment so all four active fins was then used to control the roll moment of the body

Figure 4.47: Plus and X fins configuration

4.6.1. Static Stability Analysis

The static stability of the rocket is calculated using OpenRocket. The software is used to design the rocket ,determine the stability margin and its performance. The rocket design is optimized within the software till it is made statically stable with suitable margin. A good rule of thumb is of 1-2 calibers. This also includes the shift of the cp at extreme angle of attack.

Figure 4.48: Rocket design in OpenRocket

4.6.2. CFD Analysis

For the computational fluid dynamics (CFD) analysis, Ansys 2022 is used, as a high-fidelity tool is essential for obtaining accurate aerodynamic data for rocket performance assessment. A steady-state simulation is conducted to evaluate the drag and lift forces acting on the fins. Additionally, the Direct Optimization tool in Ansys is employed for fin shape optimization, ensuring optimal aerodynamic efficiency.

The computational mesh consists of 1,427,586 elements, with an average skewness of 0.26 and an average orthogonal quality of 0.73. These mesh metrics confirm the quality and accuracy of the discretization, further supported by converged residuals. A pressure-based solver is used in conjunction with the k- turbulence model. The simulation is considered converged once the residuals drop to 0.008 for momentum equations and 0.0001 for continuity, with iterations continuing until monitored values stabilize.

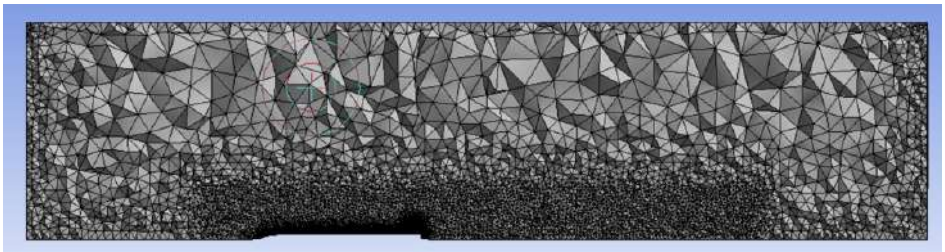

Figure 4.49: Mesh of geometrical model

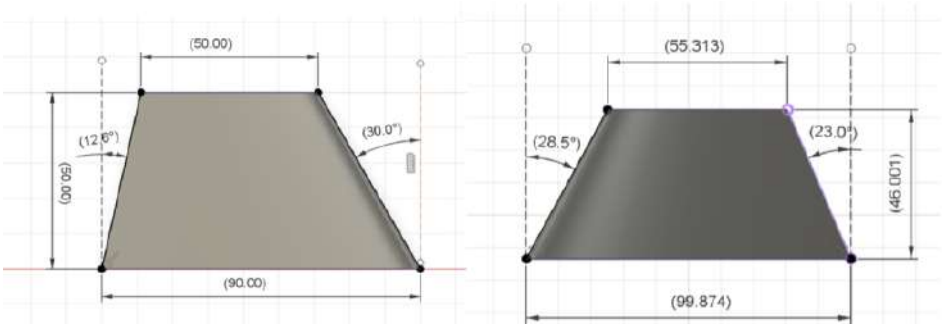

Figure 4.50: Baseline vs optimized fin

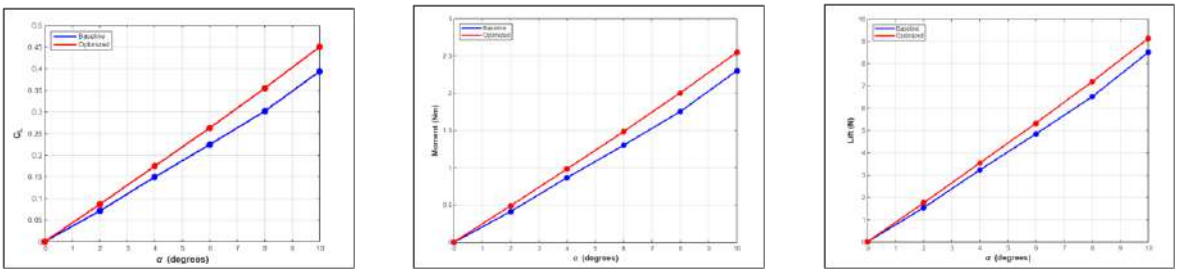

Figure 4.51: Baseline vs optimized fins property

The range of angle of attack () in the simulation is constrained by the stalling torque of the servo motor. At 10° angle of attack, the aerodynamic torque acting on the servo reaches 2.47 Nm, exceeding the servo's stalling torque of 0.51 Nm. This mechanical limitation restricts the feasible range of angles that can be analyzed for practical implementation.

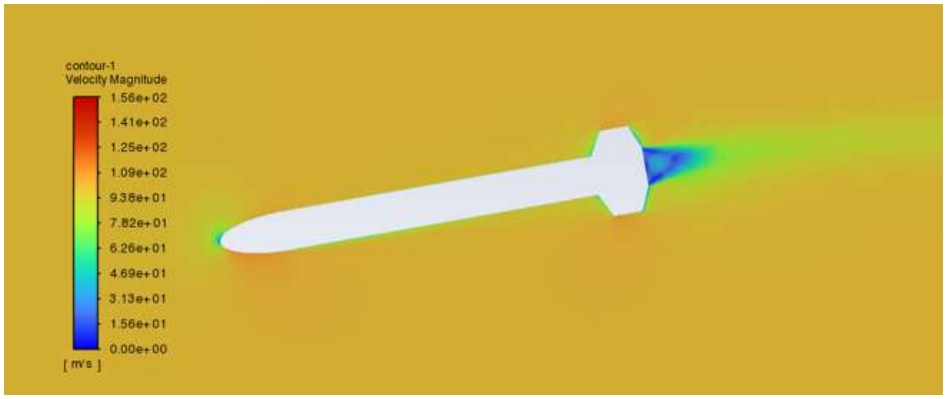

Figure 4.52: Velocity contour at 10 degree AOA

The results indicate that CL is underestimated in XFLR5 due to the absence of a viscous interactive boundary layer loop. This limitation arises because XFLR5 primarily relies on potential flow theory, which neglects the influence of boundary layer separation and viscous effects, leading to lower lift predictions compared to CFD simulations or experimental data. Additionally, a response surface has been generated based on the simulations performed for parametric optimization. This response surface can serve as a valuable tool for fin sizing in other rocket designs, enabling efficient aerodynamic analysis and design refinement. Certain optimization algorithm like L-BFGS-B and differential evolution can be implemented to speed up the optimization process.

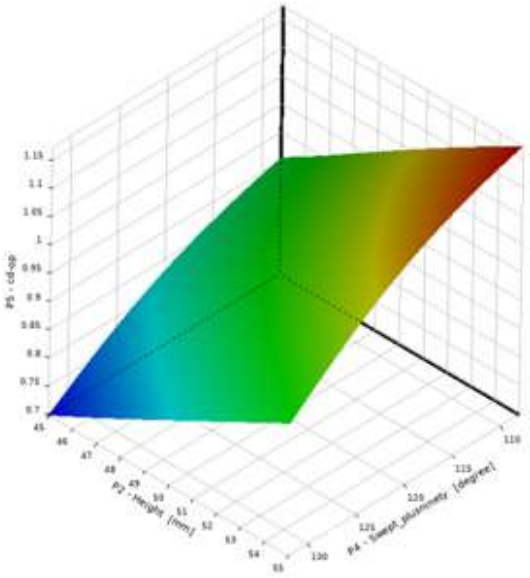

Figure 4.53: Response surface

4.7. Pitch Test Setup

The wind tunnel is used to tune the PID controller and validate the data from simulations. A setup is made that allows the movement of the model in only one axis. Two rectangular frames of plywood assembles the setup. The outer frame is attached to a frame which is stationed ahead of the wind tunnel and is connected to the inner frame through a shaft-bearing attachment. The inner frame is used to clamp the test body. The bearings are used to allow the moment of test body in only one axis. Both the pitch and yaw moment can be tested using this setup. For the test of roll moment, the nose of the body is suspended from the front of a table fan so that the roll moment can be induced. The data thus obtained from the test is further processed using MATLAB to analyze the behaviour of the model.
The speed of the wind was around 5 m/s at full power and as our objective of the test was to check the control authority, the test at even at this speed was reasonable. The test was performed by giving deflection of different angles. The response of the body after the deflection was measured using MPU6050. The measured data was the pitch angle of the body.

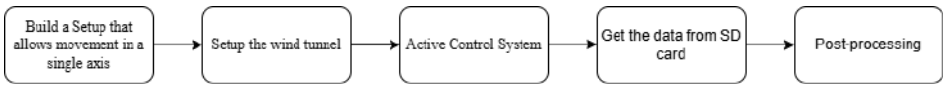

Figure 4.54: Wind tunnel flowchart

Figure 4.55: One Degree freedom setup for wind tunnel test

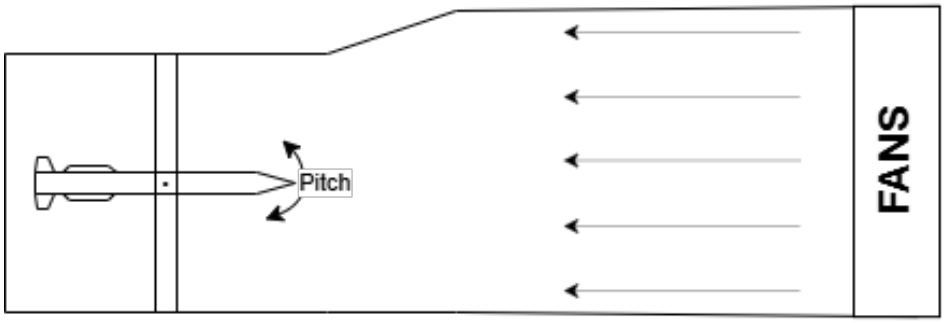

Figure 4.56: Schematic of pitch test

4.8. Roll Test Setup

Roll test of the rocket was performed using a fan only. Here, the fan blades were placed horizontal so that the rocket can be placed upright as in flight condition. The wind from the fan generated a swirl motion. This swirl wind induced roll in the rocket body and then all the four fins was used to control the roll moment.

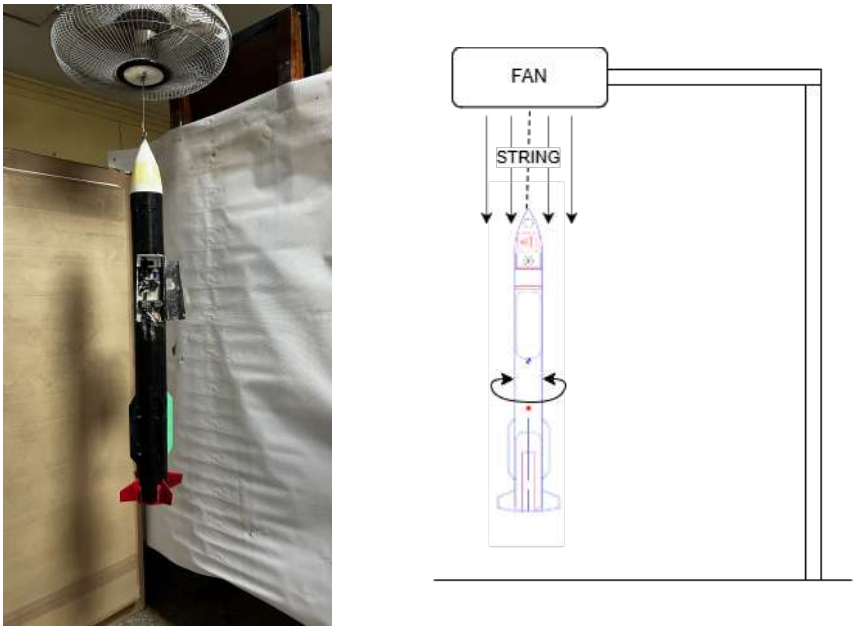

Figure 4.57: Setup for roll test

4.9. Servo Selection

Different types of servos is used in each of the flight test body: SG90 and BMS-127WV+. SG90 servo was selected due to its availability and the characterization of this servo was done to validate its capability to control the fins in flight conditions. For BMS-127WV+,

the amount of torque required for the rotation of fins in flight condition was calculated and based on the result this servo was selected. Is operating speed is 0.05 sec/60°at the operating power of 8.4V.

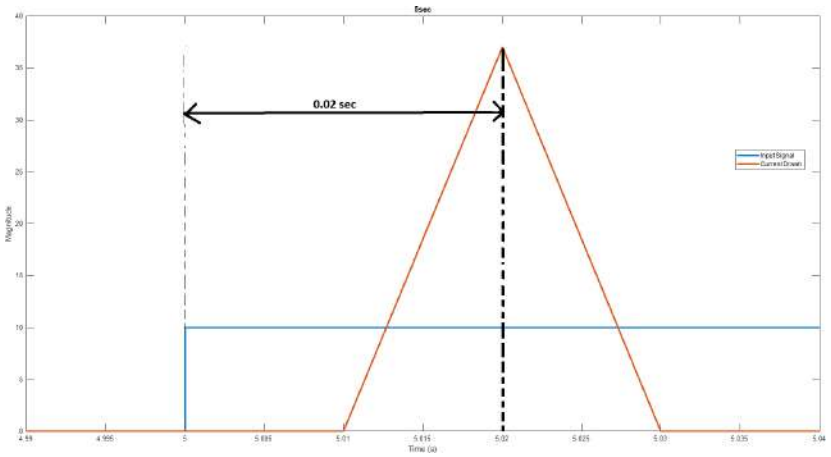

Figure 4.58: Lag response test of SG90

5. RESULTS AND DISCUSSIONS

5.1. Output

5.1.1. Static Thrust Test

The static thrust test of the KNDX propellant was performed twice. The three-grain motor was used, where the length of each grain was 50mm, with a grain diameter of 30mm and a core diameter of 10mm. Both tests showed similar results to the simulation. The test was performed with the composite motor placed inside the servo housing to check whether the housing would withstand high temperature. The test showed a positive result as there was no damage to the servo housing.

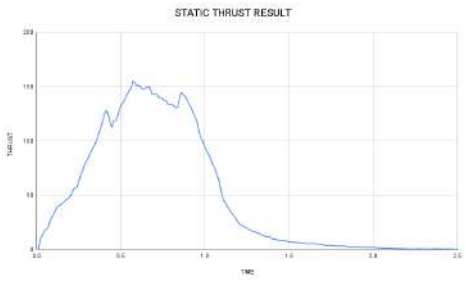

Figure 5.1: Static thrust test I

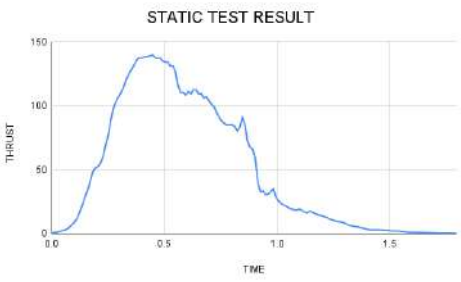

Figure 5.2: Static thrust test II

Figure 5.3: Servo housing and composite motor after static thrust test

5.1.2. Recovery Test

For Recovery of our rocket, the ejection test was performed to verify the recovery algorithm and the parachute ejection system. In one experiment, a pulley was used to lift rocket upward first, to simulate launch, and then the pulley was lowered to simulate descent. The rocket was programmed to eject after 3 meter descent from the apogee. The test was successful.

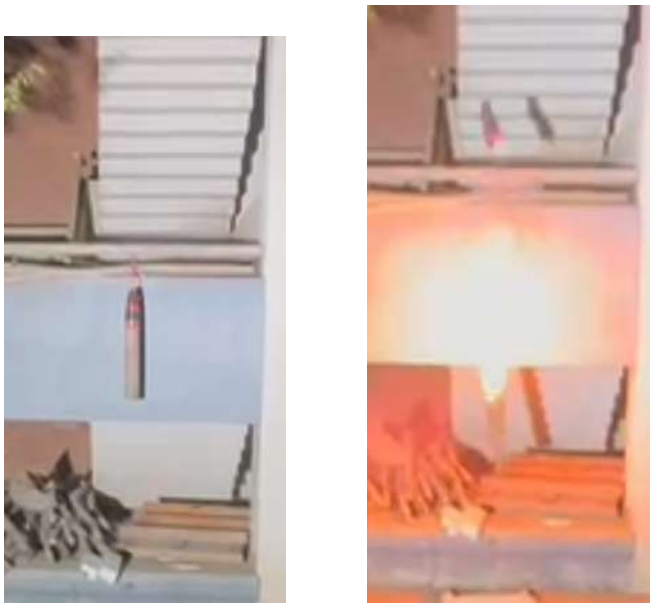

Figure 5.4: Recovery test

5.1.3. Ground Tests

5.1.3.1 Single setpoint pitch test: The wind tunnel test was performed to verify the control authority of the developed control system. During our first few tests, the body was oscillating with much higher value of oscillation with some steady-state error. However, with further tuning, we eventually reduced the error significantly with very little oscillation. Finally, our rocket's pitch inclination went from zero degree to fifteen degree with no overshoot and very less oscillation of approximately 2 degrees. The air flow speed during this was approximately 9 m/s.

major_project_report//photos/Latest/10

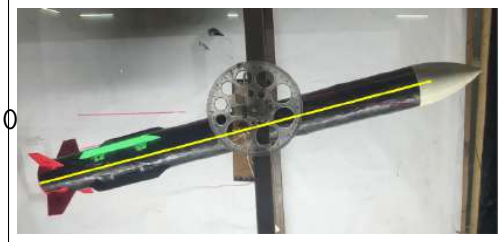

Figure 5.5: Wind tunnel test of setpoint 15^o

5.1.3.2 Multiple Setpoint Pitch Test: Four different setpoints (0^o ,15^o,0^o and 10^o) were given to the controller to maintain in series within the interval of 15 seconds. and its result was analyzed. The rocket performed well with a minimum fluctuation of 1.5^o.

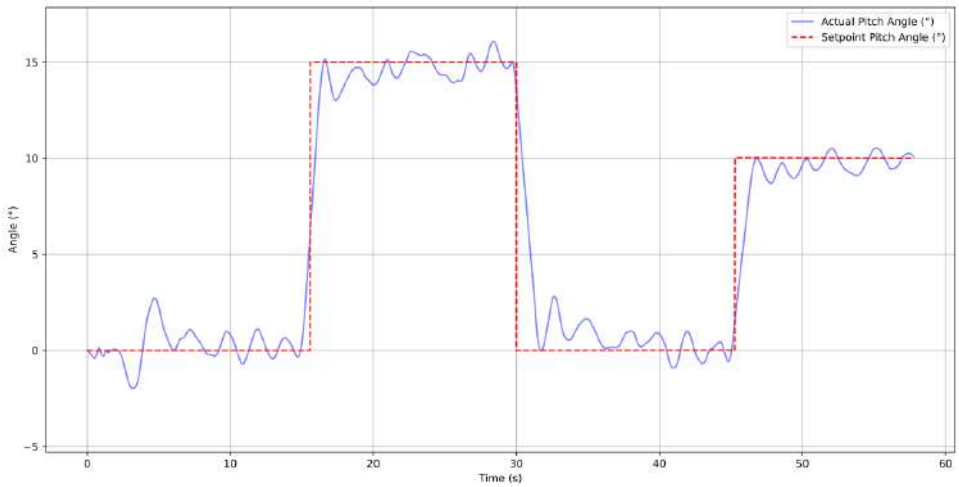

Figure 5.6: Multiple setpoint of 0^o ,15^o,0^o,10^o

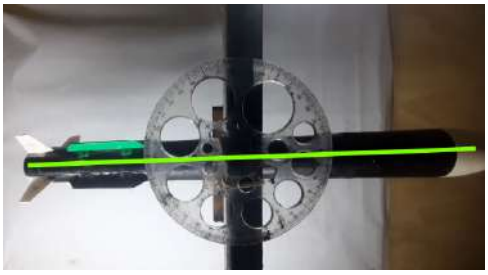

Figure 5.7: 0^o Setpoint

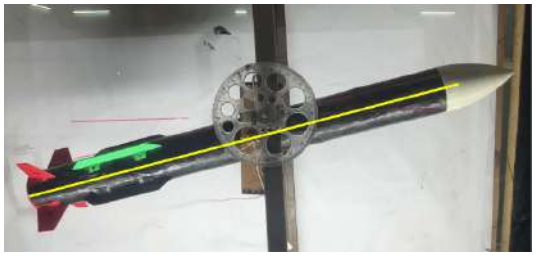

Figure 5.8: 15^o Setpoint

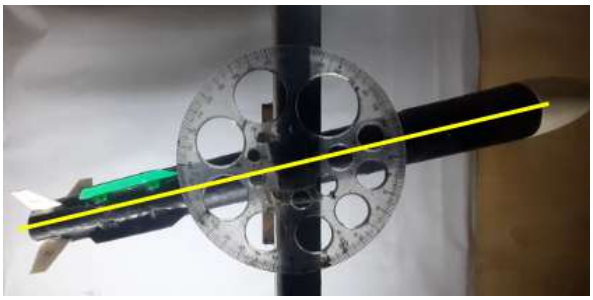

Figure 5.9: 10^o Setpoint

5.1.3.3 Roll Test: The roll test was performed using a fan, as shown in the figure, which provided a flow speed of 4m/s. Manual disturbance was provided to the roll axis of the hung rocket body to simulate and verify the robustness of our control algorithm in harsh flight conditions. After multiple tunings, we finally tuned our rocket, making it ready for the flight test. For this test, the control system was programmed to main damp the roll rate, and maintain the roll rate od $0^o/sec$.

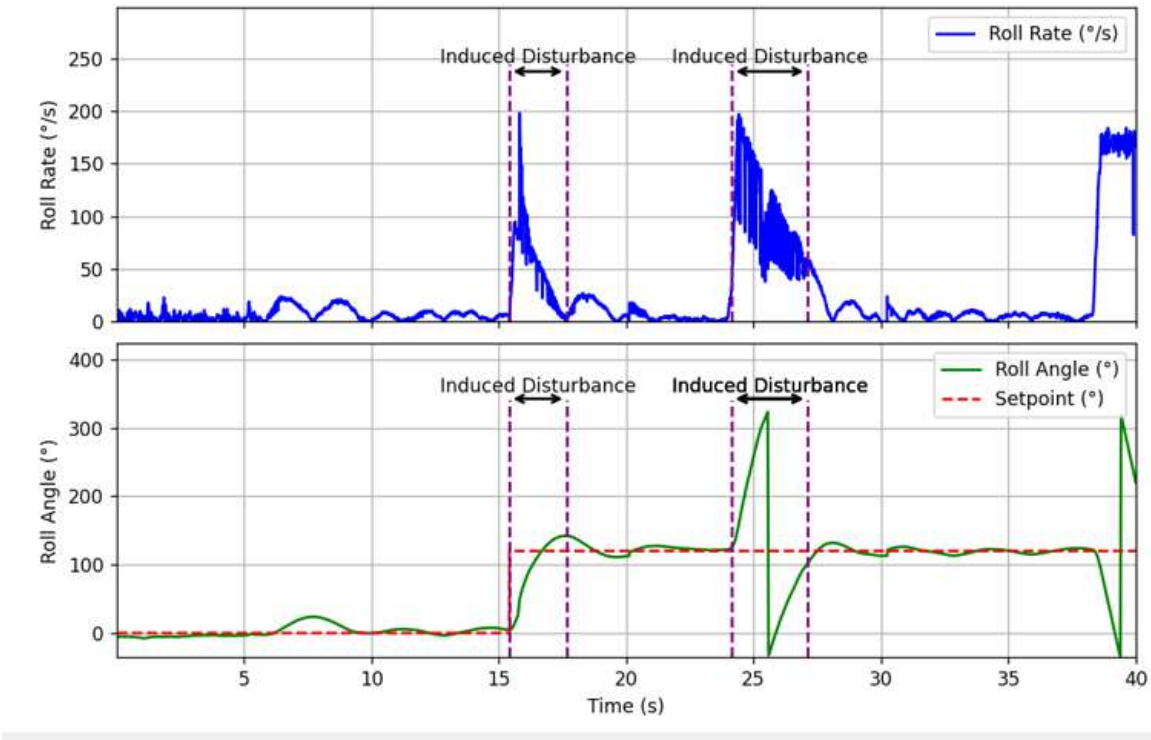

Figure 5.10: Plot Showing Control of Roll Moment 1

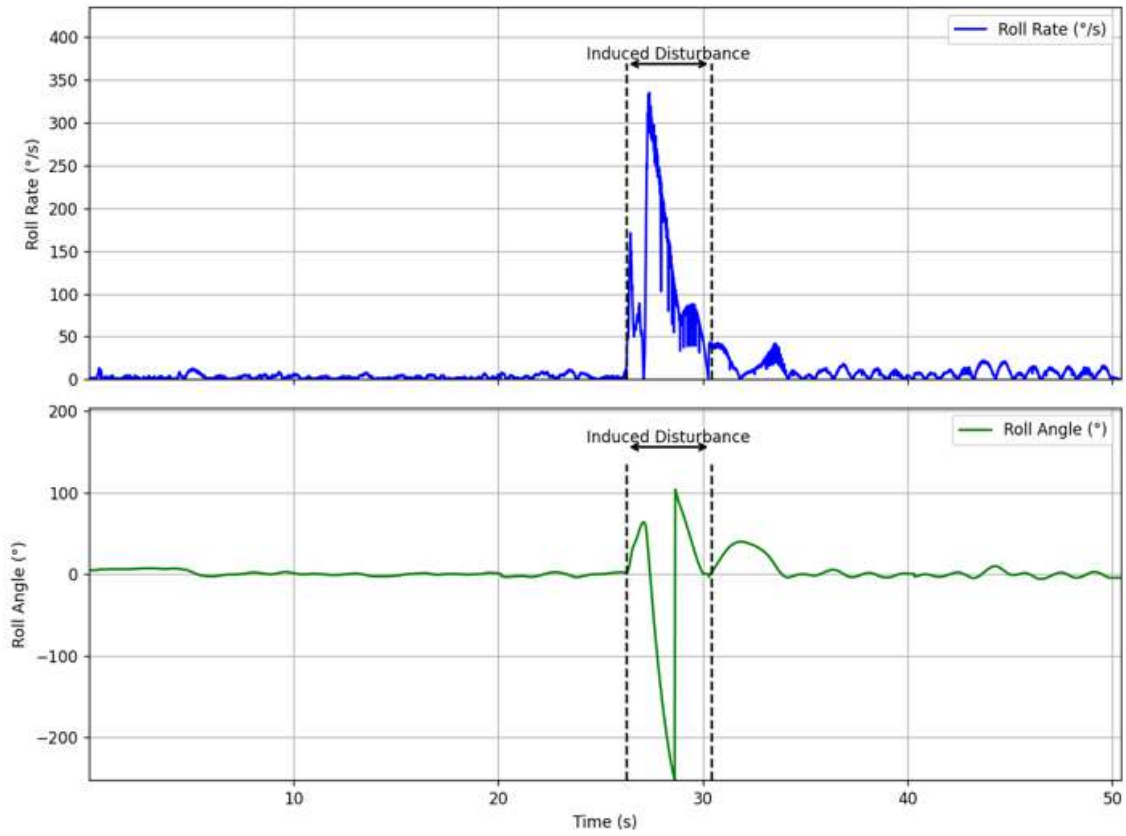

Figure 5.11: Roll Test 2

5.1.4. Flight Test

The flight test was successfully performed with the application of roll control mechanism. One flight test was performed with roll control and the other without it. Generally, roll moment gets induced during the initial stage of the flight. The main objective of the flight test was to control any induced roll moment. The control system was designed such that it would try to cancel any roll moment by controlling the roll rate of the body. Initially, there was an induced roll moment which was then canceled by the control system as can be seen in the figure 5.14. After the rocket hit the apogee, it can be seen that the roll rate has increased, this is because of the pyro ejection and uncontrollability during descent. The robustness of our control system was clearly visible as the one with control maintained it's roll angle with an error margin of just approximately 5 degrees. The recovery system successfully ignited the pyro, deploying parachute for recovery of our rocket during descent.

Figure 5.12: Rocket in lauch stand

Figure 5.13: Rocket in flight

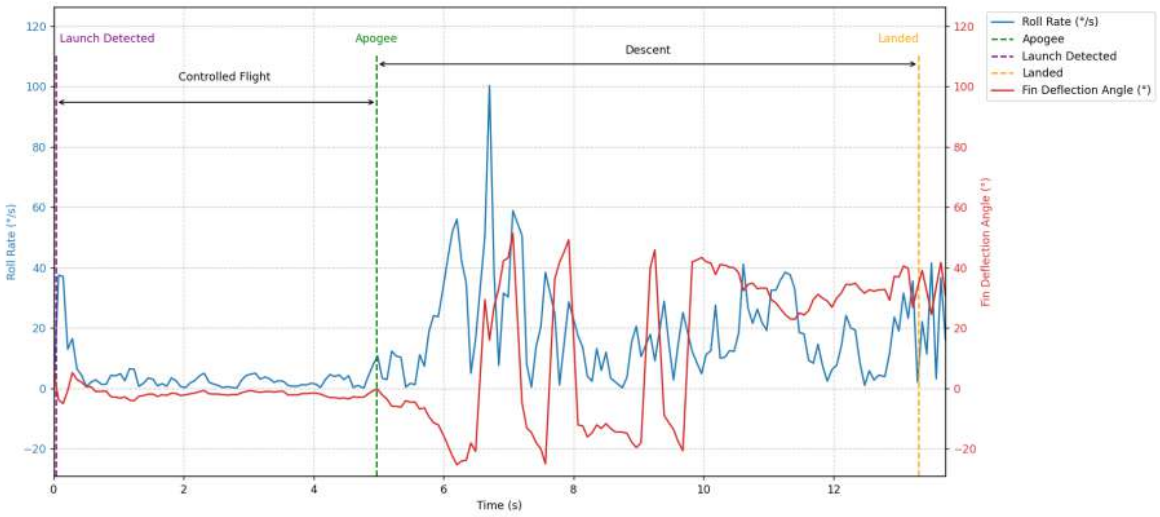

Figure 5.14: Flight test result

5.2. Problems Faced

- We faced problem regarding the test site. Properly allocated test site would make rocket flight test much easier.
- Our main flight controller(Teensy 4.1) got fired up 3 days before the flight test and we had to shift to ESP32 based microcontroller within short period of time and perform the test.
- Our project faced regulatory limitation from CAAN due to the apogee at which we will be reaching.
- We faced problem due to the frequent malfunction of micro controllers and IMU sensors.
- We encountered issues with the material to be used for the nozzle due the light weight constraints before getting hand on graphite. The static thrust test was also delayed because of this.
- We faced difficulties with the proper formulation of propellant for required burn time.

5.3. Budget Analysis

Table 5.1: Budget Analysis

S.N	Name of Particulars	Cost (NRs.)
1	Micro Controller	20,000
2	Sensors	10,000
3	PCB Fabrication	5,000
4	Power Management system	5,000
5	Communication	5,000
6	Body Fabrication	15,000
7	Propulsion	10,000
8	Recovery	5,000
10	Miscellaneous	10,000
Total		**75,000**

5.4. Gantt chart

Figure 5.15: Timeline

6. CONCLUSION AND FUTURE ENHANCEMENT

6.1. Conclusion

The flight test where only roll control was performed showed that roll moment was properly controlled. This proved that the control algorithm and mathematical model used for PID tuning worked properly. The pitch test in the wind tunnel also showed a promising result for the flight test. The wind tunnel test also verified the control algorithm. This showed that the flight test would also have been successful.
In conclusion, both the mathematical model and control algorithm of roll and pitch control were properly designed. This is valuable for future enhancement of this project.

6.2. Scope For Future enhancement

The flight test to perform pitch maneuver could be done. Also, specific pre programmed flight path could be assigned to the rocket and flight test could be done. Instead of PID control, more advanced control algorithm could be implemented. The fuel composition for the motor needs to be made so as to generate required thrust for desired amount of time to be able to perform all control moves. This would also enhance the quality of data collected which will further help to enhance the control algorithm and mathematical model.

References

[1] "Roll reversal phenomenon control in flight vehicles," *Aerospace Science and Technology*, vol. 79, pp. 413–425, 2018.

[2] A. Datye, G. Bandodkar, S. Syeda, and S. Manchkanti, "Effects of shark caved fins on altitude performance of a high-powered rocket," *2019 NCUR*, 2019.

[3] A. Datye, "Fin optimization for enhanced flight performance of an experimental rocket," in *Proceedings of The National Conference On Undergraduate Research*, 2018, pp. 5–7.

[4] G. di Pasquo, "Aerovector," Universidad Tecnológica Nacional – Regional Haedo, Tech. Rep., 2020.

[5] R. Sumathi and M. Usha, "Pitch and yaw attitude control of a rocket engine using hybrid fuzzy-pid controller," *The Open Automation and Control Systems Journal*, vol. 6, no. 1, 2014.

[6] A. B. Kisabo, A. F. Adebimpe, O. C. Okwo, and S. O. Samuel, "State-space modeling of a rocket for optimal control system design," in *Ballistics*. IntechOpen, 2019.

[7] C. Montella, "The kalman filter and related algorithms: A literature review," *Res. Gate*, pp. 1–17, 2011.

[8] M. R. Malik and D. M. Bushnell, "Role of computational fluid dynamics and wind tunnels in aeronautics r and d," Tech. Rep., 2012.

[9] D. Favier, "The role of wind tunnel experiments in cfd validation," *Encyclopedia of Aerospace Engineering*, 2010.

[10] S. Niskanen, "Openrocket technical documentation," *Development of an Open Source model rocket simulation software*, pp. 11–13, 2013.

[11] V. A. Guerrero, A. Barranco, and D. Conde, "Active control stabilization of high power rocket," 2018.

[12] G. H. Stine and B. Stine, "Handbook of model rocketry," *Wiley*, 2004.

[13] R. Galejs, "What barrowman left out," 2018.

[14] R. A. Nakka, "Solid propellant rocket motor design and testing," Ph.D. dissertation, University of Manitoba, 1984.

[15] A. F. El-Sayed, *Fundamentals of aircraft and rocket propulsion*. Springer, 2016.

[16] J. S. Barrowman, "The practical calculation of the aerodynamic characteristics of slender finned vehicles," Tech. Rep., 1967.

[17] D. Simon, *Optimal State Estimation: Kalman, H Infinity, and Nonlinear Approaches*. Wiley, 2006. [Online]. Available: https://books.google.com.np/books?id=UiMVoP_7TZkC

[18] R. E. Kalman, "A new approach to linear filtering and prediction problems," 1960.

A. APPENDIX

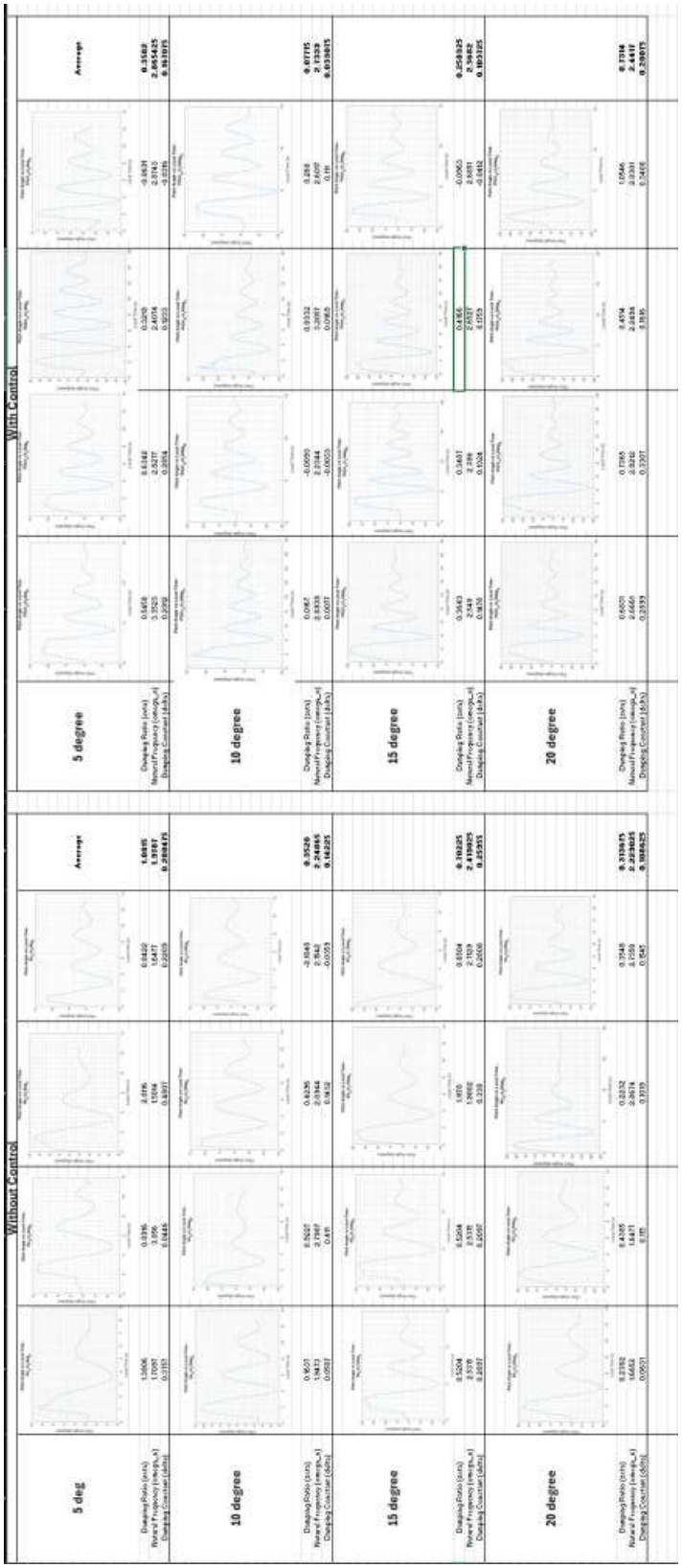

Figure A.1: Various pitch test

Figure A.2: First iteration of servo housing

Figure A.3: Trip for first flight test

Figure A.4: Propellant

Figure A.5: Getting ready for flight

Figure A.6: Properly recovered rocket

Figure A.7: Getting Ready for flight test II and III

Figure A.8: Safety precautions while working with composites

Figure A.9: Manufacturing

Figure A.10: Pitch test using laser